RESEARCH ARTICLE

Modifying TIMER to generate a slow-folding DsRed derivative for optimal use in quickly-dividing bacteria

Pavan Patel[1], Brendan J. O'Hara[2], Emily Aunins[2], Kimberly M. Davis[1]*

1 W. Harry Feinstone Department of Molecular Microbiology and Immunology, Johns Hopkins Bloomberg School of Public Health, Baltimore, Maryland, United States of America, **2** Department of Molecular Biology and Microbiology, Tufts University School of Medicine, Boston, Massachusetts, United States of America

* kdavi140@jhu.edu

Abstract

It is now well appreciated that members of pathogenic bacterial populations exhibit heterogeneity in growth rates and metabolic activity, and it is known this can impact the ability to eliminate all members of the bacterial population during antibiotic treatment. It remains unclear which pathways promote slowed bacterial growth within host tissues, primarily because it has been difficult to identify and isolate slow growing bacteria from host tissues for downstream analyses. To overcome this limitation, we have developed a novel variant of TIMER, a slow-folding fluorescent protein, named $DsRed_{42}$, to identify subsets of slowly dividing bacteria within host tissues. The original TIMER folds too slowly for fluorescence accumulation in quickly replicating bacterial species (*Escherichia coli*, *Yersinia pseudotuberculosis*), however $DsRed_{42}$ accumulates red fluorescence in late stationary phase cultures of *E. coli* and *Y. pseudotuberculosis*. We show $DsRed_{42}$ signal also accumulates during exposure to sources of nitric oxide (NO), suggesting $DsRed_{42}$ signal detects growth-arrested bacterial cells. In a mouse model of *Y. pseudotuberculosis* deep tissue infection, $DsRed_{42}$ signal was detected, and primarily accumulates in bacteria expressing markers of stationary phase growth. There was no significant overlap between $DsRed_{42}$ signal and NO-exposed subpopulations of bacteria within host tissues, suggesting NO stress was transient, allowing bacteria to recover from this stress and resume replication. This novel $DsRed_{42}$ variant represents a tool that will enable additional studies of slow-growing subpopulations of bacteria, specifically within bacterial species that quickly divide.

Author summary

We have generated a variant of TIMER that can be used to mark slow-growing subsets of *Yersinia pseudotuberculosis*, which has a relatively short division time, similar to *E. coli*. We used a combination of site-directed and random mutagenesis to generate $DsRed_{42}$, which has red fluorescent signal accumulation in post-exponential or stationary phase cells. Since this variant accumulates only red fluorescence, it is no longer a TIMER protein, and is more appropriately termed $DsRed_{42}$. We found that nitric oxide (NO) stress is

sufficient to promote $DsRed_{42}$ signal accumulation in culture, however within host tissues, $DsRed_{42}$ signal correlates with a stationary phase reporter (*dps*). These results suggest NO may cause an immediate arrest in bacterial cell division, but during growth in host tissues exposure to NO is transient, allowing bacteria to recover from this stress and resume cell division. Thus instead of indicating a response to host stressors, $DsRed_{42}$ signal accumulation within host tissues appears to identify slow-growing cells that are experiencing nutrient limitation.

Introduction

Identifying differences in the growth rates of individual cells can provide significant information in many biological systems. Quickened growth rates can indicate transformative properties in mammalian cells, indicate that specific B cell populations are expanding in response to infection or vaccination, or suggest distinct differentiation programs are occurring within cell populations during the developmental stages of an organism. For populations of bacterial cells, rapidly dividing bacteria are generally more metabolically active and thereby more susceptible to antibiotic treatments, whereas slowly dividing cells have decreased metabolic activity and are less susceptible to antibiotic treatment [1–3].

Many research groups have begun to develop tools to differentiate between faster and slower dividing cells, which enable downstream studies to identify additional differences within subpopulations. Many of these tools, such as slow-folding fluorescent proteins, were initially developed to study eukaryotic systems [4,5]. However, several of these approaches have been adapted to study bacterial populations, primarily to better understand the pathways that lead to the formation of slow-growing subsets of bacteria with reduced antibiotic susceptibility. Some bacterial tools to detect differential cell division rates include: fluorescence dilution or plasmid loss approaches [6–8]; detection of DNA replication machinery [9,10]; and differential labeling of the cell envelope to detect newly synthesized macromolecules [11,12]; which can all be used in combination with fluorescence microscopy and live imaging techniques. It has been difficult to apply these techniques to identify slow growing bacteria in the context of mammalian infection models, since many infection models are not amenable to live imaging platforms, and instead utilize endpoint analyses. Bacterial population numbers can also contract and expand dramatically during infection [13,14], which can dilute fluorescent signals or plasmids very early after inoculation and result in a complete loss of signal.

Slow-folding fluorescent proteins may offer an alternative method to identify slow growing cells within bacterial populations. TIMER is a slow-folding derivative of the tetrameric fluorescent protein, DsRed, that has been successfully used to detect differential replication rates of *Salmonella enterica* serovar Typhimurium (*S.* Typhimurium) during growth in the spleen [15]. Wild-type (WT) DsRed generates both green and red monomers during fluorescence maturation; green monomers fold more quickly than red monomers, which require an extra amidation reaction during folding [16]. The green monomeric species is also less stable, resulting in incorporation of very few (~10%) green monomers into tetrameric DsRed, and predominantly red signal [16]. In contrast, TIMER contains a S197T mutation that stabilizes the green monomeric form [4,17]. When TIMER is initially expressed, this results in an early accumulation of predominantly green monomers and green fluorescent signal. With continued translation and folding, red monomeric species are incorporated into newly formed tetramers, which generates mixed 'orange' tetramers containing both green and red monomers [17]. In fast-growing cells, cell division occurs before red monomers fold, and green signal predominates.

In slow-growing cells, red monomers are incorporated before cell division occurs; therefore mixed green and red tetramers, can be detected. To increase the fluorescent signal intensity for use in bacteria, TIMER[bac] (S4T, S197T relative to DsRed) was generated [15]. The accumulation of red fluorescent signal requires TIMER[bac] protein folding prior to cell division [15], and so the utility of this tool is dependent on the cell division rate of the cells of interest. Red TIMER[bac] signal emerges within *S*. Typhimurium dividing approximately 0.16 times/hour, or one doubling every 6 hours [15]. However, bacterial species such as *Escherichia coli* or *Yersinia pseudotuberculosis* can divide as quickly as 1.5–2 times/hour, or one doubling every 30–45 minutes, in culture [18,19]. When we began this study, it remained unclear if either TIMER or TIMER[bac] could be used to identify slow growing cells within bacterial populations that divide this rapidly, although our results and others suggest TIMER[bac] could be used [15,20,21].

Yersinia pseudotuberculosis in an enteric human pathogen that can escape the intestinal tract and replicate within deep tissue sites to form clonal extracellular clusters of bacteria called microcolonies (or pyogranulomas) [22–24]. Multiple immune cell types are recruited to the site of infection; however, bacteria continue to replicate, aided by their large arsenal of virulence factors [25–27]. Bacteria at the periphery of microcolonies respond to neutrophil contact by expressing high levels of the anti-phagocytic type-III secretion system and its associated effector proteins [24]. Peripheral bacteria also respond to and detoxify the diffusible antimicrobial gas, nitric oxide (NO), which is produced by recruited monocytes circumscribing the neutrophil layer [24,28]. NO detoxification occurs through expression of *hmp*, a nitric oxide dioxygenase, which converts antimicrobial NO to the innocuous NO_3 [29]. It remains unclear if the protective expression of *hmp* by peripheral cells comes at a fitness cost, and if this stress promotes the formation of a slow-growing subset of bacteria at the periphery of microcolonies. The preferential survival of *hmp*-expressing cells during antibiotic treatment supported this hypothesis [30], however our results here will suggest that NO exposure occurs transiently within host tissues, and that Hmp^{+} cells retain the ability to divide.

Here, we sought to generate a new TIMER variant to detect differential growth rates of *Y. pseudotuberculosis* (Yptb) within host tissues using both site-directed and random mutagenesis. This variant, DsRed[42], accumulates red fluorescent signal late in stationary phase Yptb, allowing us to detect slow-growing subsets of bacterial cells during growth in culture and within host tissues. DsRed[42] lacks green fluorescent signal, thus it is no longer a TIMER protein, but this allows us to compare red fluorescence accumulation to green fluorescent stress reporter constructs and ask if stressed cells have a heightened DsRed[42] expression. Using these constructs together, we show that NO stress is sufficient to promote DsRed[42] signal accumulation in culture; however, NO exposure within host tissues appears to be transient, and does not cause prolonged slowed growth. Instead, we detected a separate population of DsRed[42][+] bacteria within host tissues, which also have markers of stationary phase cells (*dps* expression). DsRed[42] will be a very useful tool for future studies by enabling isolation of slow growing subsets of bacteria from host tissues for downstream analyses.

Results

Site-directed and random mutagenesis were used to generate a novel TIMER variant, termed DsRed[42]

To test the hypothesis that responses to reactive nitrogen species (RNS) were sufficient to slow the growth of stressed cells, we sought to develop tools to specifically detect slow-growing subpopulations of bacteria within *Y. pseudotuberculosis* microcolonies. We focused our efforts on TIMER, since this fluorescent protein had been successfully used to identify and isolate slow-growing populations of *S*. Typhimurium from the mouse spleen [5,15].
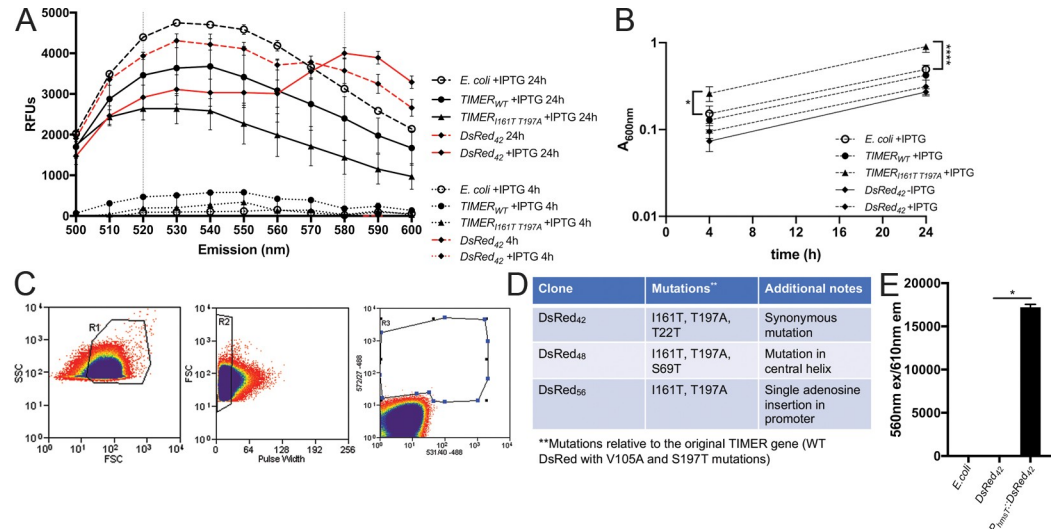
Fig 1. Site-directed and random mutagenesis were used to generate a novel TIMER variant, termed DsRed₄₂. A) Clones were grown in LB in the presence and absence of IPTG for 24 hours, shaking at 37°C. Fluorescence was detected with a spectral curve with excitation at 480nm and emission detected between 500nm-600nm. Relative fluorescence units (RFUs) represent raw values with media only background subtracted. TIMER and DsRed clones are shown alongside the non-fluorescent *E. coli* parent strain. Data represents mean of three biological replicates. B) Optical density of the indicated strains was measured by absorbance (A_{600nm}) at the indicated timepoints (hours, h). C) Gating strategy for fluorescence-activated cell sorting. FSC, SSC, and pulse width were used to select the bacterial population (within R1 and R2 gates), and cells within gate R3 were defined as red fluorescent, and were collected. D) Table summary of 4 clones selected with high red fluorescence in stationary phase *E. coli*. Clone name is shown with all mutations relative to TIMER, and additional notes about each clone. E) Red fluorescence (560nm excitation, 610nm emission) of stationary phase (24h growth) non-fluorescent DH5αλpir *E. coli* parent strain, containing DsRed₄₂ (inserted into pMMB67EH multiple cloning site), or containing P_{hmsT}::DsRed₄₂ (inserted into pMMB67EH multiple cloning site), without IPTG induction. Data represents three biological replicates. Statistics: B) Two-way ANOVA with Tukey's multiple comparison test; E) Kruskal-Wallis one-way ANOVA with Dunn's post-test; ****p < .0001, *p < .05.

TIMER was inserted into the high copy vector, pUC18, downstream of the IPTG-inducible P_{tac} promoter, and transformed into *E. coli*. *E. coli* cultures were grown 24 hours (h) in the presence of IPTG to induce TIMER expression, and fluorescence was detected by plate reader using 480nm excitation and emission detection from 500nm to 600nm to detect the incorporation of both green and red monomers into TIMER tetramers [15]. Fluorescence was not detected in exponential phase cells (4h growth), and faint green signal could be detected from bacteria late in stationary phase (24h growth). However, this green signal remained below the background signal from non-fluorescent *E. coli*, and red TIMER signal did not accumulate (**Fig 1A and 1B**). We then generated a TIMER$_{I161T\ T197A}$ variant, which should lack green fluorescent signal and accumulate red signal more quickly due to quickened folding kinetics [1]. Because TIMER$_{I161T\ T197A}$ lacks green fluorescence, this is no longer a TIMER protein, but we have left the TIMER name here to depict it was derived from TIMER. We were hoping faster folding would allow us to detect red TIMER$_{I161T\ T197A}$ fluorescence accumulation in post-exponential or stationary phase cells, and eliminating the green monomeric species would allow us to use green fluorescent stress reporters alongside TIMER$_{I161T\ T197A}$. However, TIMER$_{I161T\ T197A}$ also did not have detectable red fluorescent signal after 24 h growth with IPTG induction (**Fig 1A and 1B**). Additionally, we quantified expression of TIMER$_{I161T\ T197A}$ in a low copy vector, pMMB67EH, which we typically use for reporters in our mouse model of infection. We did not observe detectable fluorescence in stationary phase (24h growth) *E. coli* or *Y. pseudotuberculosis* (Yptb), in the presence or absence of IPTG induction (**S1 Fig**).

We hypothesized this lack of red fluorescence accumulation was because the folding of red monomeric TIMER$_{I161T\ T197A}$ was still too slow, relative to the doubling times of Yptb and *E. coli*. Therefore, we used the TIMER$_{I161T\ T197A}$ construct as a template for random mutagenesis, to specifically isolate variants that have red fluorescence accumulation in stationary phase cells. Since these variants have only red fluorescence, they will be referred to as DsRed variants from here on. Variants were inserted into pUC18, transformed into *E. coli*, and transformants were grown for 24h with IPTG. Non-fluorescent *E. coli* cultures were grown in parallel to define the threshold for fluorescence detection during cell sorting. Forward scatter (FSC), side scatter (SSC) and pulse width detection were used to identify individual bacterial cells, and we collected bacteria with detectable 572nm emission (gate R3) (**Fig 1C**). Collected bacteria (approximately 200 cells) were plated for single colonies, and 192 colonies were screened for red fluorescence during growth in the presence of IPTG by plate reader. 26 clones had detectable red fluorescence in stationary phase (24h growth) compared to exponential phase (4h growth); one clone, DsRed$_{42}$, is shown as a representative (**Fig 1A and 1B**). Red fluorescence emerged between 16h and 20h of growth in the presence of IPTG (**S2A–S2C Fig**); some red fluorescence was also detected without IPTG induction (**Figs 1A and S2D**), likely due to the high copy number of pUC18. The 26 clones were sequenced, and their DsRed sequences represented three different 'types', numbered based on the well number of the first observed clone. Three of the sequenced clones were the DsRed$_{42}$ type, with a T22T synonymous mutation (ACC—> ACA) that is predicted to increase translation efficiency [31]; one clone was the DsRed$_{48}$ type, with a S69T mutation in the central helix that likely impacts chromophore maturation, since it is adjacent to chromophore residues 66–68 [11]; and the other 22 clones were the DsRed$_{56}$ type, which contain a TIMER$_{I161T\ T197A}$ gene with a single adenosine insertion upstream of the start codon, likely resulting in increased transcript levels (**Fig 1D**). Of these three clone types, DsRed$_{42}$ and DsRed$_{56}$ had high red fluorescent signal in stationary phase, but the signal from DsRed$_{48}$ was dim in comparison (**S2D Fig**). Because of its bright signal and confirmed mutation within the gene, we selected the DsRed$_{42}$ clone for additional experiments.

We then sought to move DsRed$_{42}$ into the low copy vector pMMB67EH, which is stably maintained during mouse infection [24,28]. Insertion of DsRed$_{42}$ into the pMMB67EH multiple cloning site (MCS) did not result in detectable fluorescence despite the upstream P_{tac} promoter, so we also inserted P_{hmsT}, the promoter for the diguanylate cyclase *hmsT*, upstream of DsRed$_{42}$. Our *Y. pseudotuberculosis* strain (IP2666) naturally contains a disrupted Fur binding site in P_{hmsT}, which should result in low, constitutive transcription of genes downstream of P_{hmsT} [32,33]. P_{hmsT} was sufficient to promote the accumulation of red DsRed$_{42}$ monomers in stationary phase *E. coli* (24h growth), in the absence of IPTG induction (**Fig 1E**).

After generating DsRed$_{42}$, we also tested another TIMER variant, TIMER^{bac} [15]. This variant had high fluorescence in *Y. pseudotuberculosis*, but expression from a low-copy vector (pSC101) resulted in significant growth inhibition, and overnight cultures only reached 2.5 x 10^7 CFU compared to 1 x 10^{10} CFU for WT *Y. pseudotuberculosis* strains. For future studies, we could modify this TIMER^{bac} construct by changing the promoter or vector, or modify the ribosomal binding site or start codon to reduce translation initiation, to generate a construct with strong fluorescence that does not inhibit growth [34–36]. This TIMER^{bac} variant folds into green and red monomeric species, which provides an important internal control for levels of expression, however the presence of the green monomeric species means we would not be able to assess stress levels with green fluorescent reporters alongside TIMER^{bac}. Additional reporters could be generated with blue fluorescent protein variants to use alongside TIMER^{bac} [20,37], and mCherry-derived TIMER variants also exist with emission that transitions from

blue to red fluorescence [38], however we chose to move forward with $DsRed_{42}$ and green fluorescent reporters for this study.

$DsRed_{42}$ accumulates red, but not green fluorescence in stationary phase *Y. pseudotuberculosis*

The P_{hmsT}::$DsRed_{42}$ construct was then transformed into WT *Y. pseudotuberculosis* (Yptb) to determine if $DsRed_{42}$ signal accumulation could be detected in stationary phase Yptb. Initially, we utilized IPTG induction, and detected fluorescent signal accumulation using a plate reader alongside bacterial growth, based on absorbance. Bacterial cultures were in stationary phase between 16h (hours) and 24h growth; bacterial numbers were similar between the strains, although $DsRed_{42}$ had a slightly higher absorbance value after 24h of growth (**Fig 2A**). A significant increase in $DsRed_{42}$ signal was detected after 16h of growth in the presence of IPTG (**Fig 2B**). $DsRed_{42}$ signal continued to increase between 20h and 24h of growth in the presence of IPTG, confirming $DsRed_{42}$ signal accumulates in late stationary phase Yptb. We hoped to utilize green fluorescent reporters alongside our $DsRed_{42}$ construct, so it was important to determine if the $DsRed_{42}$ construct would produce interfering fluorescence across green wavelengths. Despite high red signal accumulation, no significant green fluorescence was detected (**Fig 2C**). We then asked whether $DsRed_{42}$ signal would accumulate in the absence of IPTG-induction, since we would not be inducing with IPTG in our mouse model of deep tissue
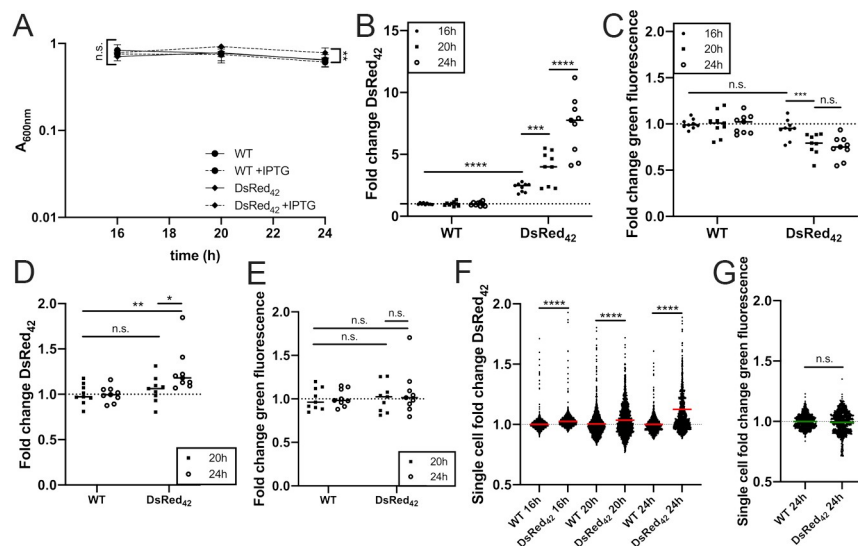

Fig 2. $DsRed_{42}$ accumulates red, but not green fluorescence in stationary phase *Y. pseudotuberculosis*. WT IP2666 Yptb and P_{hmsT}::$DsRed_{42}$ Yptb strains were grown in 96 well plates at 37°C with shaking, in the presence or absence of 1mM IPTG, for the indicated timepoints (hours: h). Fluorescence was detected by plate reader and fluorescence microscopy. A) Optical density of the indicated strains was measured by absorbance (A_{600nm}) at the indicated timepoints (hours, h). B) Plate reader detection of $DsRed_{42}$ signal accumulation with IPTG induction. Dots: biological replicates. C) Plate reader detection of green fluorescence with IPTG induction, same samples as B). Dots: biological replicates. D) Plate reader detection of $DsRed_{42}$ signal accumulation without IPTG. Dots: biological replicates. E) Plate reader detection of green fluorescence without IPTG, same samples as D). Dots: biological replicates. F) Fluorescence microscopy to detect $DsRed_{42}$ signal within individual bacterial cells, grown for the indicated times in the absence of IPTG. Dots: individual cells. G) Green fluorescence from bacterial cells shown in F). Fold change: signal relative to non-fluorescent WT IP2666, grown alongside $DsRed_{42}$ strains under the same conditions and timepoints. Data represents 9 biological replicates for each condition. Dotted lines: baseline value of non-fluorescent WT IP2666 cells. Bars: mean values. Statistics: A)-E) Two-way ANOVA with Tukey's multiple comparison test; E) Kruskal-Wallis one-way ANOVA with Dunn's post-test; F) Mann-Whitney; ****p < .0001, ***p < .001, **p < .01, *p < .05, n.s.: not-significant.

infection, and found that $DsRed_{42}$ signal could be detected after 24h growth in LB (**Fig 2D**). We also confirmed that cells lacked green fluorescent signal at this timepoint (**Fig 2E**).

Plate reader detection represents fluorescent values averaged across all cells within a well of a 96-well plate. To determine if there was variability in $DsRed_{42}$ signal accumulation within individual bacterial cells in these samples, we used fluorescence microscopy to detect fluorescence at the single cell-level. There was a significant increase in the mean $DsRed_{42}$ signal after 16h, 20h, and 24h growth relative to non-fluorescent WT cells, but this was most apparent at 24h growth (**Fig 2F**). The observed variability across the bacterial population suggests that subsets of cells are truly slow-growing, $DsRed_{42}^{+}$, at each of these timepoints, while cells lacking $DsRed_{42}$ signal accumulation may remain more metabolically active. We also confirmed that cells lacked green fluorescent signal after 24h growth, again suggesting that GFP reporters can be used alongside $TIMER_{42}$ (**Fig 2G**). Collectively, these data indicate that $DsRed_{42}$ signal accumulates late in stationary phase Yptb, between 16h and 24h of culture, and that the $DsRed_{42}$ construct lacks green fluorescent signal. Many DsRed variants exist, including DsRed-Express2, and it remains unclear if $DsRed_{42}$ has advantages relative to this DsRed variant or others [39]. DsRed-Express2 is bright, photostable, and fast folding, and does retain green monomeric signal [39]; $DsRed_{42}$ is relatively dim, likely similar to DsRed, but lacks green fluorescence, which could be an advantage of $DsRed_{42}$.

$DsRed_{42}$ is detected within the host spleen at 72h p.i.

To quantify the relative $DsRed_{42}$ signal accumulation within individual bacterial cells, we transformed $DsRed_{42}$-expressing Yptb (P_{hmsT}::$DsRed_{42}$) with a plasmid that constitutively-expresses GFP [24,28]. To determine when $DsRed_{42}$ signal accumulated during bacterial growth in the spleen, we intravenously infected C57BL/6 mice with this GFP^{+} $DsRed_{42}$ strain and harvested spleens at 48h and 72h post-inoculation (p.i.) to detect $DsRed_{42}$ signal. $DsRed_{42}$ signal was not detected in microcolonies at 48h p.i., but was detectable at 72h p.i. (**Fig 3A**). To determine if $DsRed_{42}$ signal accumulated in a specific spatial location within microcolonies, we compared the ratio of $DsRed_{42}$/GFP signal intensity at the geometric centroid and periphery of individual microcolonies (**Fig 3B**). There was not a significant difference in the relative $DsRed_{42}$ signal at the centroid or periphery, suggesting $DsRed_{42}$ accumulation does not occur in a specific spatial location across microcolonies. We also compared the relative $DsRed_{42}$ signal at the centroid and periphery of each microcolony, and found a slight positive correlation in the two signals (**Fig 3C**). This shows that higher centroid signal correlates with higher periphery signal, and further suggests that on average, the $DsRed_{42}$ signal isn't specifically enriched at either the centroid or the periphery. However, $DsRed_{42}$ signal accumulation also did not appear uniform across microcolonies, which could suggest that specific subsets of cells may be transitioning to a slowed growth phenotype.

$DsRed_{42}$ signal accumulates after stationary phase markers

To determine if there are specific subsets of Yptb that exhibit $DsRed_{42}$ accumulation and slowed growth, we compared $DsRed_{42}$ signal to expression from several different fluorescent reporters. We began by testing $DsRed_{42}$ alongside two different *dps* reporter constructs, which should also detect slow-growing subsets of cells. *dps* expression occurs when bacteria transition into stationary phase, and *dps* gene expression has been used extensively as a marker of slowed growth [40]. However, Dps protein levels are regulated at the transcriptional, post-transcriptional, and translational levels by multiple pathways, suggesting that a *dps* transcriptional reporter alone may not be sufficient to identify slow growing cells, necessitating a tool like $DsRed_{42}$ [41]. We generated two *dps* reporters: P_{dps}::*gfp* and P_{dps}::*gfp-ssrA*, where the *dps*
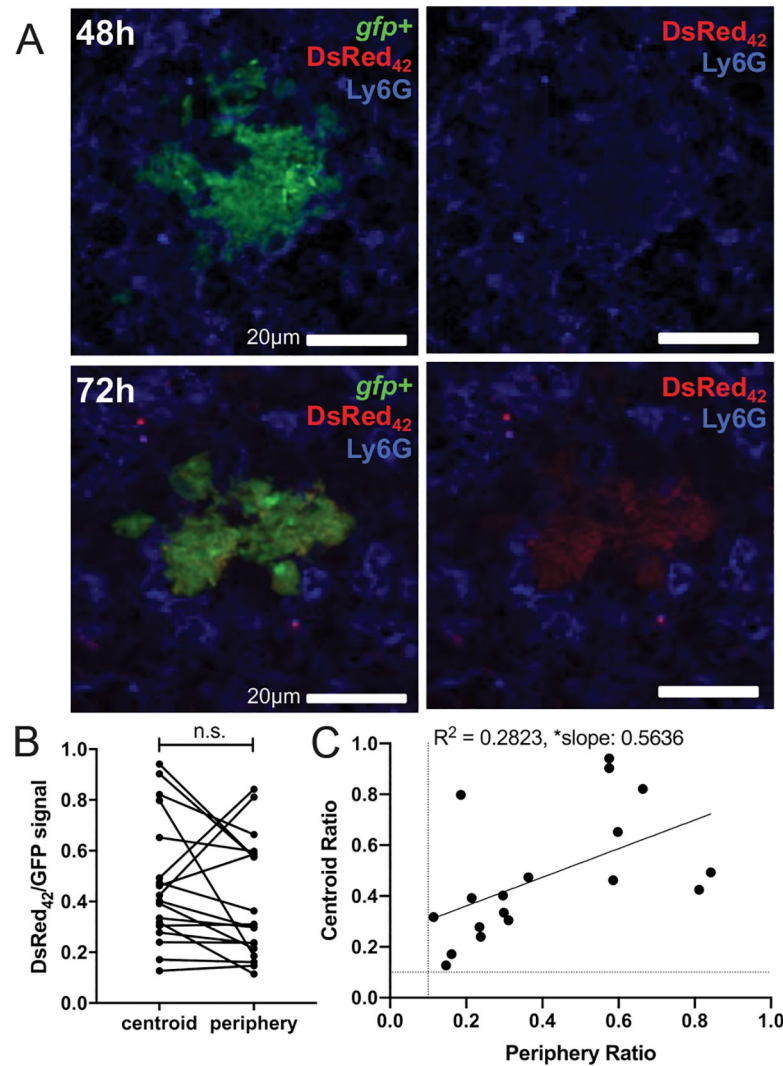
Fig 3. DsRed$_{42}$ is detected within the host spleen at 72h p.i. C57BL/6 mice were infected intravenously with the DsRed$_{42}$ (P_{hmsT}::$DsRed_{42}$) GFP^{+} strain for the indicated timepoints post-inoculation (p.i.) A) Representative images are shown at 48h and 72h as merged images (left), and without the green channel (right). Tissues were also stained for neutrophils (Ly6G). B) DsRed$_{42}$ signal intensity was divided by GFP signal intensity (DsRed$_{42}$/GFP signal) at the centroid and periphery. Each dot: individual microcolony. Lines connect centroid and periphery values from the same microcolony. C) The DsRed$_{42}$/GFP ratio at the centroid was plotted relative to the periphery value for each microcolony. Each dot: individual microcolony. Dotted lines: threshold for signal detection; only microcolonies with detectable DsRed$_{42}$ signal were included in the analysis. Statistics: B) Wilcoxon-matched pairs; C) linear regression with R^2 value and slope of best-fit line; *p $<$ .05, n.s.: not significant. Significantly non-zero slope indicates values are correlated. Tissues were analyzed from 4 mice for 48h and 6 mice for 72h timepoints, collected from two independent experiments; between 3 to 15 microcolonies were analyzed for each spleen, from a single cross-section of each tissue.

promoter is fused to stable and destabilized *gfp*, respectively [42,43]. This destabilized version of *gfp* has a half-life of approximately 37 minutes in culture, compared to approximately 147 minutes for stable *gfp*, indicating the destabilized GFP signal will depict recent transcriptional changes (**S3 Fig**). *dps* reporters were transformed into DsRed$_{42}$-expressing Yptb (DsRed$_{42}$ P_{dps}::*gfp* or DsRed$_{42}$ P_{dps}::*gfp-ssrA*), individual colonies were inoculated into 96 well plates, and fluorescent signals were detected over time. Expression of the stable *dps* reporter was first detected after 5h growth, and remained relatively steady for about 12h, until we saw a gradual
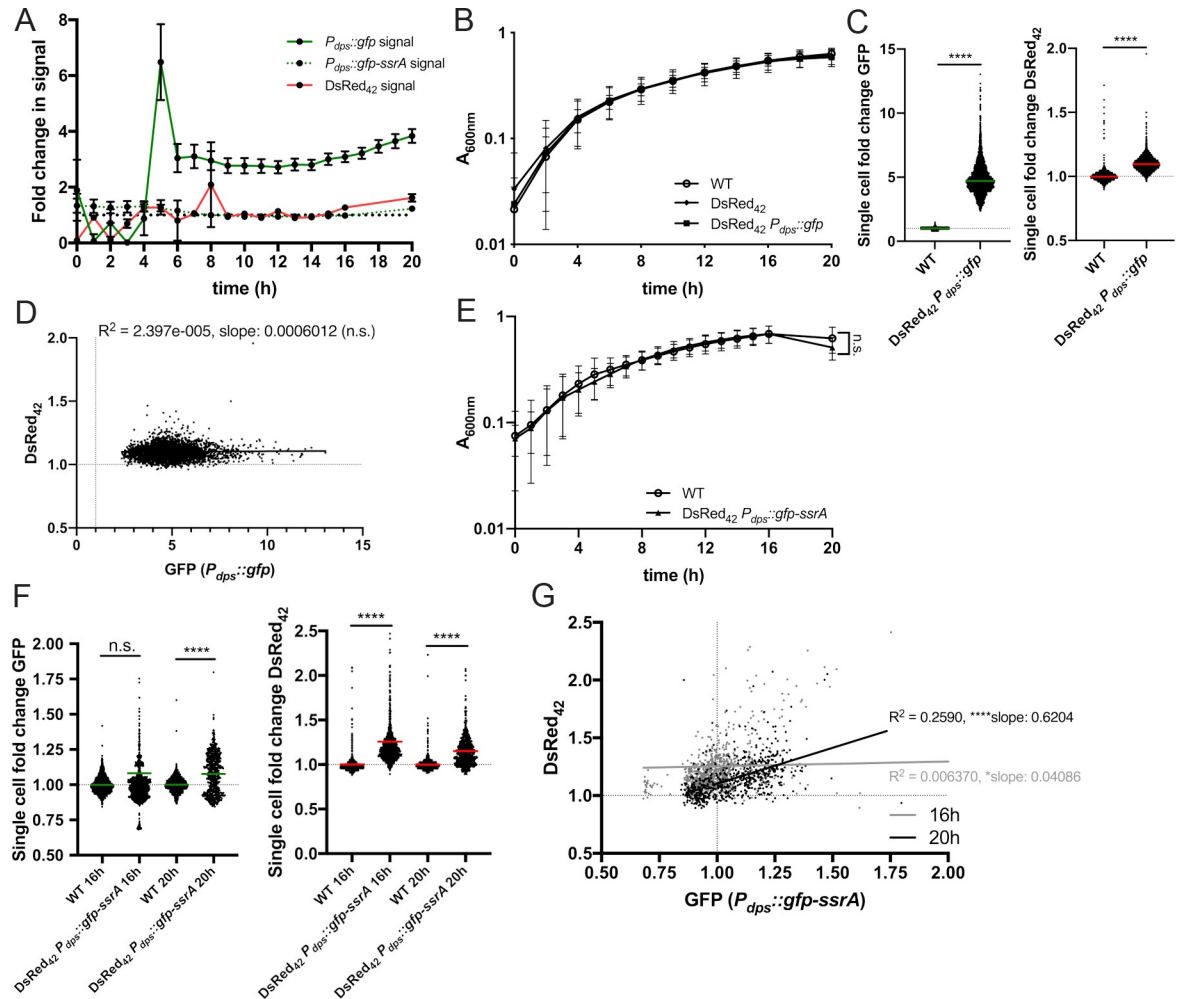
Fig 4. DsRed$_{42}$ signal accumulates after stationary phase markers. P_{dps}::gfp DsRed$_{42}$, P_{dps}::gfp-$ssrA$ DsRed$_{42}$ and WT strains were grown in 96 well plates at 37°C under standing conditions for the indicated timepoints, and fluorescence was detected by plate reader and fluorescence microscopy. A) Timecourse of fluorescent signal detection by plate reader, shown as fold change relative to non-fluorescent WT cells. DsRed$_{42}$ data shown from the P_{dps}::gfp-$ssrA$ DsRed$_{42}$ strain, to compare with P_{dps}::gfp-$ssrA$ reporter signal; very similar results were obtained with DsRed$_{42}$ signal from the P_{dps}::gfp DsRed$_{42}$ strain. Plate reader data represents 15 biological replicates for each strain. B) Optical density of the indicated strains was measured by absorbance (A$_{600nm}$) at the indicated timepoints (hours, h). C) Fold change GFP and DsRed$_{42}$ within individual bacteria quantified by fluorescence microscopy. Indicated strains were grown 16 hours. D) Correlation plot of fold change in DsRed$_{42}$ and GFP signals from bacteria in C). Dots: individual cells. E) Optical density of the indicated strains was measured by absorbance (A$_{600nm}$) at the indicated timepoints (hours, h). F) Fold change GFP and DsRed$_{42}$ within individual bacteria quantified by fluorescence microscopy. Indicated strains were grown 16 or 20 hours. G) Correlation plot of fold change in DsRed$_{42}$ and GFP signals from bacteria in F). Dots: individual cells. Dotted lines: baseline value of non-fluorescent WT cells. Microscopy data represents 4 biological replicates for each strain and condition. Statistics: C) Mann-Whitney; D) & G) linear regression with R^2 value and slope of best-fit line; E) Two-way ANOVA with Tukey's multiple comparison test; F) Kruskal-Wallis one-way ANOVA with Dunn's post-test; ****p < .0001, *p < .05, n.s.: not-significant. Significantly non-zero slope indicates values are correlated.

increase in signal (**Fig 4A**). The signal increase after 5h growth clearly occurred prior to stationary phase, based on absorbance data (**Fig 4B**). In contrast, the destabilized *dps* reporter had very little fluorescence until 20h growth, which was similar to the pattern with DsRed$_{42}$ signal accumulation in the same strain background (**Fig 4A**). 20h growth clearly represented stationary phase based on absorbance data (**Fig 4B and 4E**). DsRed$_{42}$ signal accumulation was very similar in both strain backgrounds; only DsRed$_{42}$ signal in DsRed$_{42}$ P_{dps}::gfp-$ssrA$ is shown to directly compare the two signals in this strain. These data suggested that the stable

P_{dps}::*gfp* reporter signal accumulates prior to the stationary phase transition, and that the destabilized P_{dps}::*gfp-ssrA* reporter is more accurately detecting slow growing cells.

There was a significant increase in both P_{dps}::*gfp* and $DsRed_{42}$ signal after 16h growth, a timepoint that represented stationary phase (**Fig 4B**), as detected by fluorescence microscopy (**Fig 4C**), however there was no correlation between these two signals within individual bacteria (**Fig 4D**), likely due to the early accumulation of stable GFP prior to the stationary phase transition. However, with the $DsRed_{42}$ P_{dps}::*gfp-ssrA* strain, significant GFP signal was not detected until 20h growth by fluorescence microscopy, while $DsRed_{42}$ was detected at both 16h and 20h growth (**Fig 4F**). There was a significant correlation between P_{dps}::*gfp-ssrA* and $DsRed_{42}$ signal at 20h growth, suggesting these reporters are detecting the same subsets of cells, and are behaving similarly at this late timepoint (**Fig 4G**). For additional information about statistical analyses for correlations, see Materials and Methods below. Collectively, this indicates that both *dps* and $DsRed_{42}$ can be used to identify slow growing cells. However, *dps* signal detection is heavily dependent on the stability of GFP, and an early increase in *gfp* transcripts prior to the transition into stationary phase can lead to prolonged signal detection. $DsRed_{42}$ signal accumulation is detected well after this point, and likely means that $DsRed_{42}$ can be used to detect cells much later in stationary phase.

$DsRed_{42}$ signal accumulation correlates with *hmp* expression during exposure to acidified nitrite

We then sought to determine if the response to reactive nitrogen species (RNS) is sufficient to slow the growth of cells and promote $DsRed_{42}$ signal accumulation, since we observe bacterial responses to this stress during growth in the spleen [24,28]. To determine if RNS were sufficient to promote $DsRed_{42}$ signal accumulation, we first used the acidified nitrite method of generating nitric oxide (NO), where $NaNO_2$ is added to acidified LB (pH 5.5) [24,28,44]. The 2.5mM $NaNO_2$ concentration was known to inhibit growth and promote high levels of *hmp* expression, whereas 0.25mM represents a sub-inhibitory concentration [28]. *hmp* and $DsRed_{42}$ fluorescence were detected within individual cells by fluorescence microscopy. At 2h post-treatment, all concentrations of $NaNO_2$ promoted *hmp* expression, and there was significantly higher *hmp* expression with the highest concentration, 2.5mM (**Fig 5A**). $DsRed_{42}$ signal accumulation was also detected following exposure to 1mM and 2.5mM $NaNO_2$, but $DsRed_{42}$ signal was highest with 1mM $NaNO_2$ (**Fig 5B**). $DsRed_{42}$ and *hmp* signals were correlated during 1mM $NaNO_2$ treatment, but 2.5mM $NaNO_2$ resulted in a significant negative correlation, suggesting this high concentration was impacting bacterial viability due to high levels of stress (**Fig 5C**). At 4h post-treatment, the highest *hmp* reporter expression was detected with the 1mM intermediate dose, and the *hmp* signal had decreased with the 2.5mM dose, again suggestive of high levels of stress (**Fig 5D**). $DsRed_{42}$ signal was detected with all three doses, and was highest with 2.5mM (**Fig 5E**). However, there was an interesting divergence in the 1mM population, where both $DsRed_{42}^+$ and $DsRed_{42}^-$ cells were observed, suggesting that some cells may have recovered from stress and resumed growth resulting in a loss of $DsRed_{42}$ signal (**Fig 5E**). We observed a significant positive correlation between $DsRed_{42}$ and *hmp* signals with the low 0.25mM and intermediate 1mM doses at this timepoint, but no correlation with the highest 2.5mM dose (**Fig 5F**). We believe this decrease in *hmp* signal and lack of correlation between *hmp* and $DsRed_{42}$ signals with the 2.5mM dose could suggest additional impacts of this stress, potentially on either transcriptional activity or transcript stability within these cells, resulting a more pronounced impact on *hmp* reporter signal and less impact on $DsRed_{42}$ signal, which is predominantly impacted by protein folding. Collectively, these results show that acidified nitrite is sufficient to promote $DsRed_{42}$ signal accumulation, and suggest $DsRed_{42}$ can be used to detect growth-arrested cells.
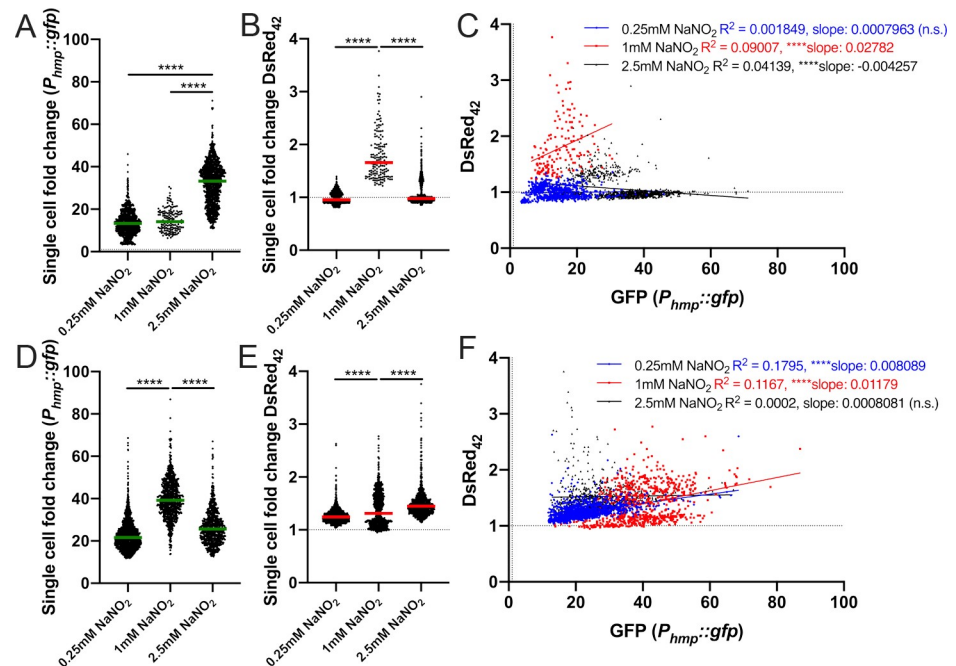
Fig 5. DsRed$_{42}$ signal accumulation correlates with *hmp* expression during exposure to acidified nitrite. P_{hmp}::*gfp* DsRed$_{42}$ and WT strains were grown in LB pH5.5 in 96 well plates at 37°C with shaking, with the indicated concentrations of NaNO$_2$, for either 2h (panels A-C) or 4h (panels D-F). Fluorescence of individual bacteria was detected by fluorescence microscopy. Fold change in signal is shown relative to non-fluorescent WT bacteria treated under the same conditions (dotted lines). A) GFP fluorescence after 2h treatment. B) DsRed$_{42}$ fluorescence after 2h treatment. C) Correlation plot of fold change in DsRed$_{42}$ and GFP signals from bacteria in A) and B). D) GFP fluorescence after 4h treatment. E) DsRed$_{42}$ fluorescence after 4h treatment. F) Correlation plot of fold change in DsRed$_{42}$ and GFP signals from bacteria in D) and E). Dots: individual cells. Dotted lines: baseline value of non-fluorescent WT cells. Microscopy data represents 4 biological replicates for each strain and condition. Statistics: A), B), D), E): Kruskal-Wallis one-way ANOVA with Dunn's post-test; C) & F): linear regression with R^2 value and slope of best-fit line; ****$p < .0001$, *$p < .05$, n.s.: not-significant. Significantly non-zero slope indicates values are correlated.

https://doi.org/10.1371/journal.ppat.1009284.g005

NO stress is sufficient to promote DsRed$_{42}$ signal accumulation

The results with acidified nitrite suggest that RNS are sufficient to promote DsRed$_{42}$ signal accumulation, but to truly show nitric oxide (NO) exposure is sufficient, we performed experiments with the DETA-NONOate NO donor compound. Cultures of the DsRed$_{42}$ P_{hmp}::*gfp* and DsRed$_{42}$ P_{hmp}::*gfp-ssrA* strains were exposed to 2.5mM DETA-NONOate for 4h, and fluorescence microscopy was used to detect fluorescent signals within individual bacterial cells. The 2.5mM dose was chosen for these experiments based on our previous studies, which showed this dose is sufficient to promote *hmp* reporter expression [24,28,45]. We also confirmed that 2.5mM DETA-NONOate significantly inhibited growth of the DsRed$_{42}$ P_{hmp}::*gfp* strain, which would allow us to determine if growth inhibition by the NO donor was sufficient to promote DsRed$_{42}$ signal accumulation (**Fig 6A**). Treatment with the NO donor compound resulted in high levels of *hmp* reporter expression (**Fig 6B**), and DsRed$_{42}$ signal accumulation (**Fig 6C**). The P_{hmp}::*gfp* strain was used here as a control to detect the amount of red fluorescence in NO-treated bacteria that contained GFP but lacked DsRed$_{42}$, and we confirmed that DsRed$_{42}$ signal was significantly above the baseline fluorescence of this control strain (**Fig 6C**). We detected significantly higher fluorescent signals with the DsRed$_{42}$ P_{hmp}::*gfp* strain, however all strains had significant increased *hmp* reporter expression, and both DsRed$_{42}$ strains had red fluorescence above baseline in response to NO. DsRed$_{42}$ and *hmp* signals were significantly correlated
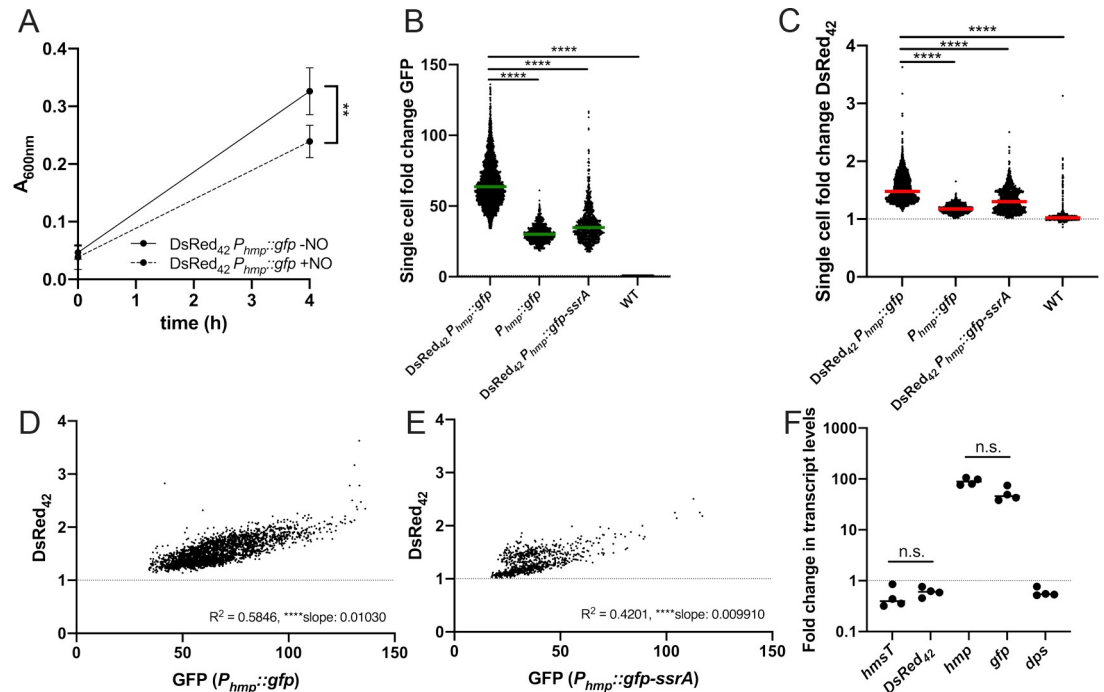
Fig 6. NO stress is sufficient to promote DsRed$_{42}$ signal accumulation. P_{hmp}::*gfp* DsRed$_{42}$, P_{hmp}::*gfp-ssrA* DsRed$_{42}$, P_{hmp}::*gfp*, and WT strains were grown in LB in 96 well plates at 37°C with shaking, with 2.5mM DETA-NONOate for 4h. A) Optical density of P_{hmp}::*gfp* DsRed$_{42}$ in the presence (+NO) and absence (-NO) of DETA-NONOate was measured by absorbance (A$_{600nm}$) at time 0h and 4h post-treatment (hours, h). B) GFP fluorescence of individual bacteria of the indicated strains was detected by fluorescence microscopy. Fold change in signal is shown relative to non-fluorescent WT bacteria treated under the same conditions (dotted lines). C) DsRed$_{42}$ fluorescence of bacteria shown in B). D) Correlation plot of fold change in DsRed$_{42}$ and GFP signals from bacteria in B) and C), P_{hmp}::*gfp* DsRed$_{42}$ strain. E) Correlation plot of fold change in DsRed$_{42}$ and GFP signals from bacteria in B) and C), P_{hmp}::*gfp-ssrA* DsRed$_{42}$ strain. Dots: individual cells. Dotted lines: baseline value of non-fluorescent WT cells. Microscopy data represents 5 biological replicates for each strain and condition. F) qRT-PCR detection of the indicated transcripts (x-axis) in P_{hmp}::*gfp* DsRed$_{42}$ bacteria during DETA-NONOate exposure, using conditions described above. Dots: individual replicates. Fold change in transcript levels relative to untreated WT cells. Four biological replicates are shown. Statistics: A) Two-way ANOVA with Tukey's multiple comparison test; B), C), F): Kruskal-Wallis one-way ANOVA with Dunn's post-test; D)- E): linear regression with R^2 value and slope of best-fit line; ****p < .0001, **p < .01, n.s.: not-significant. Significantly non-zero slope indicates values are correlated.

for both the stable reporter strain (**Fig 6D**) and the unstable reporter strain (**Fig 6E**), showing that NO is sufficient to promote DsRed$_{42}$ signal accumulation.

We also performed qRT-PCR with the DsRed$_{42}$ P_{hmp}::*gfp* strain to confirm that DsRed$_{42}$ signal accumulation in response to NO was not due to an increase in DsRed$_{42}$ transcript levels, and to verify that *hmsT* was not increasing in transcript levels during NO exposure, since this promoter was used to drive DsRed$_{42}$ expression. DsRed$_{42}$ P_{hmp}::*gfp* cells were exposed to 2.5mM DETA-NONOate for 4h and transcripts were detected by qPCR. DsRed$_{42}$ and *hmsT* transcript levels were not impacted by NO, and high levels of both *hmp* and *gfp* transcripts were detected, consistent with DsRed$_{42}$ accumulation as a result of protein folding, and *gfp* expression as a result of transcription downstream of P_{hmp} (**Fig 6F**). We also quantified *dps* transcript levels to determine if these increased in response to NO, and found there was no change in *dps* expression in response to NO (**Fig 6F**). These results provide additional insight into the mechanism of NO-mediated stress, and suggest the response to NO is sufficient to arrest cell division, but not promote a stationary phase transition. This is consistent with published results showing NO disrupts cell division by arresting assembly of the FtsZ cytokinetic ring [46,47].

DsRed$_{42}$ signal correlates with *dps* expression *in vivo*

We then asked whether there was a correlation between DsRed$_{42}$ signal accumulation and either *dps* or *hmp* reporter expression during growth within host tissues. C57BL/6 mice were inoculated intravenously with either the DsRed$_{42}$ P_{dps}::*gfp* or DsRed$_{42}$ P_{hmp}::*gfp* strains, and spleens were harvested at 72h p.i. to visualize reporter expression by fluorescence microscopy. At 72h p.i., some microcolonies had detectable DsRed$_{42}$ signal accumulation (DsRed$_{42}$$^+$), while other microcolonies lacked DsRed$_{42}$ signal (DsRed$_{42}$$^-$). This was also observed in initial experiments with the GFP$^+$ DsRed$_{42}$ strain, and only DsRed$_{42}$$^+$ microcolonies were analyzed in **Fig 3**. We hypothesized that larger microcolonies may run out of nutrients, which then slows growth, and results in DsRed$_{42}$ signal accumulation. We compared the areas of microcolonies that had or lacked DsRed$_{42}$ signal, and found that generally the DsRed$_{42}$$^+$ microcolonies were indeed larger (**Fig 7A**).
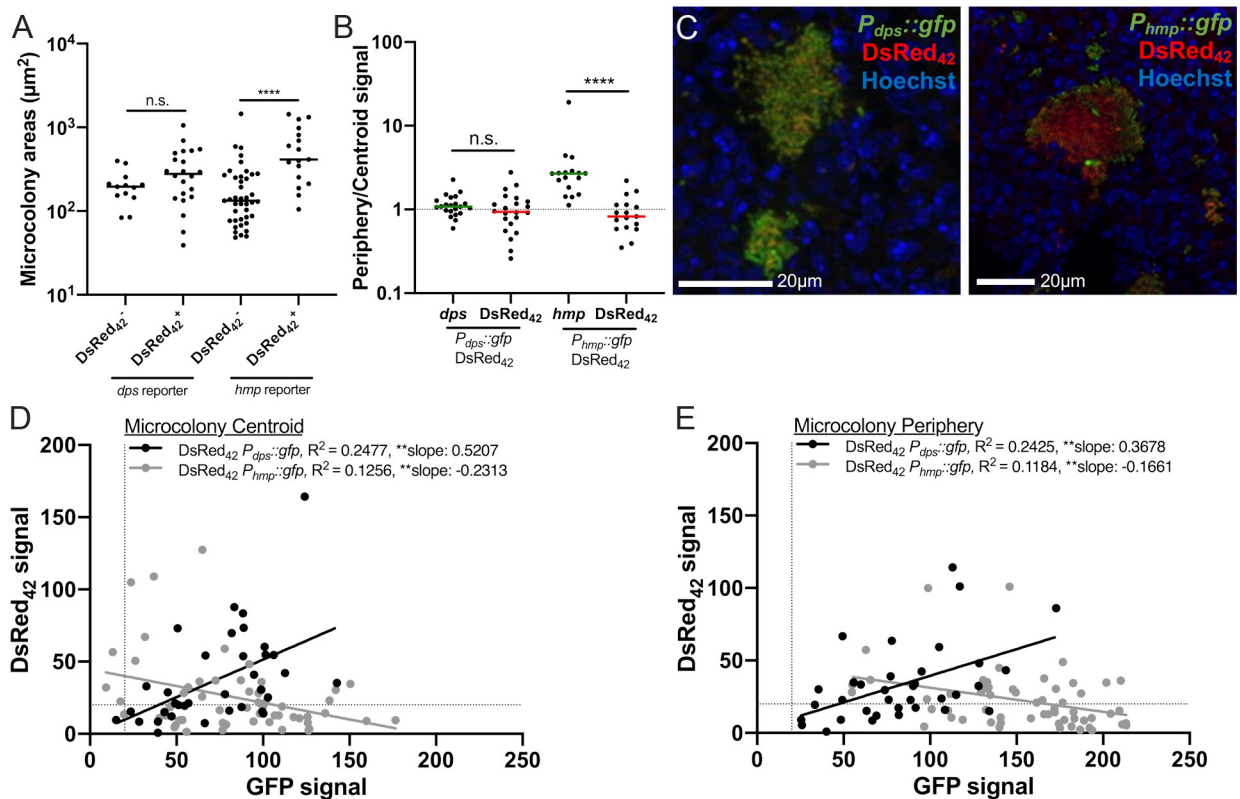

Fig 7. DsRed$_{42}$ signal correlates with *dps* expression *in vivo*. C57BL/6 mice were infected intravenously with the DsRed$_{42}$ (P_{hmsT}::*DsRed$_{42}$*) P_{dps}::*gfp* or DsRed$_{42}$ P_{hmp}::*gfp* strain for 72h, and spleens were harvested for fluorescence microscopy. A) Areas of individual microcolonies, separated based on whether TIMER$_{42}$ signal was detectable above background (DsRed$_{42}$$^+$) or undetectable (DsRed$_{42}$$^-$). Data with the DsRed$_{42}$ P_{dps}::*gfp* strain (*dps* reporter) and DsRed$_{42}$ P_{hmp}::*gfp* strain (*hmp* reporter) is shown. B) Peripheral fluorescent signal intensity was divided by centroid fluorescent intensity for each reporter (x-axis). At each spatial location, *dps* or *hmp* reporter signal was detected alongside DsRed$_{42}$ signal, to compare their signal intensities directly. Data represent microcolonies defined as DsRed$_{42}$$^+$. Dotted line: value of 1, where signal is equivalent at the centroid and periphery (no spatial patterning). C) Representative images. D) DsRed$_{42}$ signal was plotted relative to either *dps* or *hmp* reporter signal to determine if the signal intensities were correlated at the centroid of microcolonies. All microcolonies detected within tissues are included (those defined as DsRed$_{42}$$^+$ and DsRed$_{42}$$^-$). D) DsRed$_{42}$ signal was plotted relative to either *dps* or *hmp* reporter signal to determine if the signal intensities were correlated at the periphery of microcolonies. Each dot: individual microcolony. Dotted lines: threshold for signal detection. Statistics: A)- B) Wilcoxon-matched pairs; D)-E) linear regression with R^2 value and slope of best-fit line; $^{**}p < .01$, $^*p < .05$, n. s.: not significant. Significantly non-zero slope indicates values are correlated. Tissues were analyzed from 5 mice per infection, collected from two independent experiments; between 2 to 18 microcolonies were analyzed for each spleen, from a single cross-section of each tissue.

https://doi.org/10.1371/journal.ppat.1009284.g007

We then asked whether *dps* or *hmp* reporter signal correlated with DsRed$_{42}$ signal accumulation within these tissues. We first compared the ratio of *dps* and DsRed$_{42}$ signal at the periphery and centroid of microcolonies and found the signal intensity of each of these reporters looked very similar (**Fig 7B**). In comparison with DsRed$_{42}$, *hmp* reporter signal was significantly enriched at the periphery (**Fig 7B**). This *hmp* reporter signal pattern was consistent with our previously published results [24,28,45] but suggested that NO stress was not significantly slowing bacterial growth within host tissues, based on DsRed$_{42}$ signal accumulation in some, but not all, peripheral cells. Representative images indicate there was substantial overlap between *dps* and DsRed$_{42}$ signals, and that *hmp* and DsRed$_{42}$ are detecting distinct subsets of bacteria (**Fig 7C**). To further analyze the relationship between these signals, we compared the DsRed$_{42}$ and GFP signals at microcolony centroids (**Fig 7D**) and microcolony peripheries (**Fig 7E**). For each individual microcolony spatial location, the relative DsRed$_{42}$ and GFP signals are plotted on the Y- and X-axis respectively, to determine if there is a linkage between the two values by linear regression (see Materials and Methods below). At both the centroid and periphery, we found a significant positive correlation between DsRed$_{42}$ and *dps* reporter signal, however we found a significant negative correlation between DsRed$_{42}$ and *hmp* reporter signal. This supports the conclusion that *dps* and DsRed$_{42}$ are marking the same subsets of bacteria within host tissues, but suggests that *hmp* and DsRed$_{42}$ are detecting distinct subsets. This suggests that at 72h p.i., there is a subset of slow-growing Yptb at the interior of microcolonies, and also suggests that NO stress may not be sufficient to cause prolonged growth arrest within host tissues. It is also possible that changes in oxygen tension levels or DsRed$_{42}$ expression levels *in vivo* could be impacting fluorescence accumulation, and this should be explored in future studies.

DsRed$_{42}$ signal dissipates after initial responses to NO, suggesting recovery occurs *in vivo*

We were surprised to find that NO stress did not correlate with DsRed$_{42}$ signal accumulation within host tissues, and hypothesized this could be due to temporal differences in when bacteria were exposed to NO and when tissues were collected. We believe that bacteria respond to NO much earlier during infection (approximately 48h p.i., [24,30]), and it was possible that bacteria were no longer actively responding to stress. We returned to the acidified nitrite method of introducing NO stress, since this likely results in an initial burst of NO, and then slower NO generation [44]. We exposed the DsRed$_{42}$ P_{hmp}::*gfp* cells to the indicated concentrations of NaNO$_2$ in LB pH5.5, and measured absorbance (A$_{600nm}$) and reporter signal by fluorescence, in a plate reader over time. Consistent with the predicted initial burst of NO release, we initially observed growth arrest after treatment followed by slowed growth (**Fig 8A**). There was a significant increase in *hmp* reporter signal after 1h treatment that continued to increase over the course of 8h (**Fig 8B**). However, DsRed$_{42}$ signal accumulation was consistent with an initial arrest of the cell population followed by recovery and resumed growth, based on significantly higher DsRed$_{42}$ signal accumulation with 1mM treatment relative to 0.25mM treatment at 2h and 4h post-treatment, and a return to baseline levels 6h after the initial exposure to acidified nitrite (**Fig 8C**). Consistent with this DsRed$_{42}$ result, growth also appeared to resume at these timepoints in cultures, based on absorbance (**Fig 8A**).

NO exposure has recently been shown to arrest bacterial cell division through disruption of cytokinesis machinery, and so it was expected that DsRed$_{42}$ signal would accumulate in growth-arrested, NO-exposed, bacteria [47]. The lack of correlation between the two signals during growth in tissue was unexpected, and suggested that NO stress may have occurred much earlier during infection than the 72h timepoint. To test this hypothesis, we generated
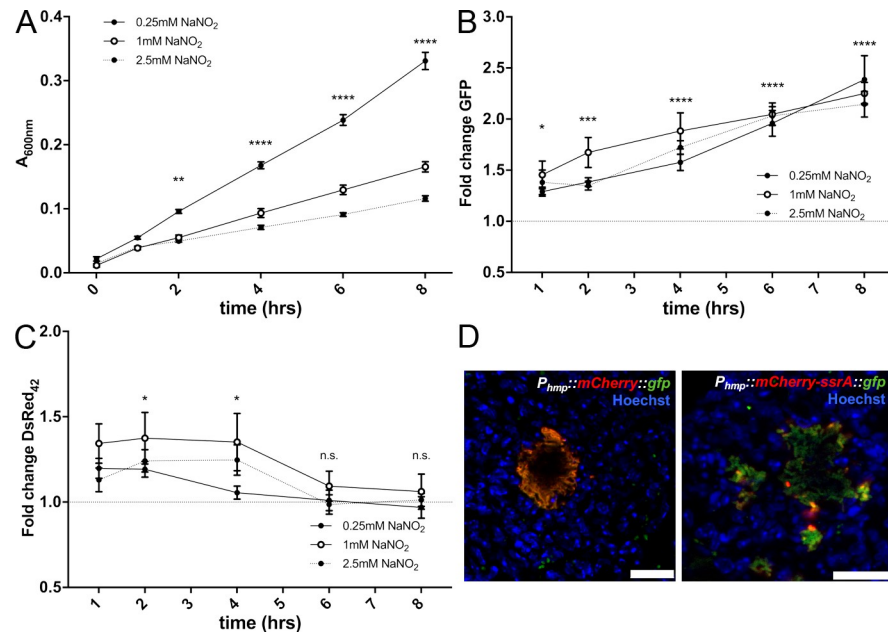
Fig 8. DsRed$_{42}$ signal dissipates after initial responses to NO, suggesting recovery occurs *in vivo*. P_{hmp}::*gfp* DsRed$_{42}$ and WT strains were grown in LB pH5.5 in 96 well plates at 37˚C with shaking, with the indicated concentrations of NaNO$_2$, for the indicated timepoints. A) Optical density of the P_{hmp}::*gfp* DsRed$_{42}$ strain was measured by absorbance (A$_{600nm}$) over time (hours, hrs), in a plate reader. B) *hmp* reporter expression (GFP signal) was detected over time by plate reader. Fold change is relative to WT non-fluorescent samples grown under the same conditions. C) DsRed$_{42}$ signal was detected over time by plate reader. Fold change is relative to WT non-fluorescent samples grown under the same conditions. D) C57BL/6 mice were infected intravenously with strains containing either the P_{hmp}::*mCherry*::*gfp* or P_{hmp}::*mCherry-ssrA*::*gfp* reporter constructs, and spleens were harvested for fluorescence microscopy at 72h p.i. Representative images are shown. Nine biological replicates are shown for plate reader data with mean and standard deviation. Statistics: A)-C): Two-way ANOVA with Tukey's multiple comparison test; ****p < .0001, ***p < .001, **p < .01, *p < .05, n.s.: not-significant. Statistics shown represent: A) and C) pair-wise comparisons between 0.25mM and 1mM treatment conditions; B) comparison between 1mM treatment and untreated cells.

constructs that contained combinations of stable and unstable fluorescent protein genes with expression driven by the P_{hmp} promoter. P_{hmp}::*mCherry*::*gfp* was a control construct generated with stable mCherry and stable GFP proteins, and we confirmed these signals overlapped during growth in tissue (**Fig 8D**). The P_{hmp}::*mCherry-ssrA*::*gfp* construct contained destabilized mCherry [30] and stable GFP, to allow us to detect bacteria that had responded to NO as some point during infection (GFP$^+$) compared to bacteria that were actively responding to NO when the tissue was harvested and fixed (mCherry$^+$). Using this reporter, we found very few bacterial cells were actively responding to NO when tissue was harvested (**Fig 8D**), suggesting that other cells may have responded to NO, recovered, and resumed growth, explaining why they no longer exhibited DsRed$_{42}$ signal accumulation. Instead, DsRed$_{42}$ signal accumulation is clearly marking an interior subset of bacteria, that are likely experiencing nutrient limitation at this late timepoint post-inoculation.

Discussion

In this study, we sought to modify TIMER to detect slow-growing bacteria within host tissues, with a goal of generating a tool to enable future studies of slow-growing bacterial populations. The DsRed$_{42}$ variant has been tested in *E. coli* and *Y. pseudotuberculosis*; the signal accumulates late in stationary phase in both of these quickly-replicating Gram-negative organisms. DsRed$_{42}$ signal was detected within host tissues, and is also visible within cultured individual

cells. However, the fold change quantification we used here indicate that the signal is some-times dim, so non-fluorescent cells need to be included as a control for all assays to define $DsRed_{42}^{+}$ cells. $DsRed_{42}$ could potentially be used directly in other Gram-negative species, or used as a template for random mutagenesis to select an optimized $DsRed_{42}$ variant in another system. Additional rounds of random mutagenesis and sorting could also be used to select for a brighter $DsRed_{42}$ variant, as done with other DsRed variants [39,48,49], and again, this may be needed to apply $DsRed_{42}$ to other bacterial systems. We believe the signal generated with $DsRed_{42}$ is sufficient to isolate expressing cells from host tissues, and plan to analyze these cells in future experiments to better understand the pathways promoting slowed bacterial growth. Additional recent applications of fluorescence dilution approaches could also be applied in our model to isolate stressed, slow-growing subsets of bacteria [50–52].

Fluorescence signal accumulation requires folding prior to cell division events, and so additional variants that fold more quickly could lead to increased signal accumulation. We have shown here that $DsRed_{42}$ signal accumulation in response to NO is likely due to protein folding during an arrest in cell division, and not changes in transcript level, based on similar *$DsRed_{42}$* transcript levels after NO donor addition (**Fig 6F**). However, it does remain somewhat unclear why the T22T synonymous mutation (ACC➔ACA) is sufficient to promote $DsRed_{42}$ signal accumulation in stationary phase cells. We initially thought this change may result in use of a more favorable threonine codon (ACA), but the original threonine codon (ACC) is used more frequently across the *Y. pseudotuberculosis* genome [53]. Instead, we believe the ACA codon may increase the stability of $DsRed_{42}$ mRNA, leading to increased levels of translation of the $DsRed_{42}$ variant relative to $TIMER_{I161T\ T197A}$, based on the predicted influence of an ACC➔ ACA change in *E. coli* [31]. These results in *E. coli* suggest that protein levels correlate better with mRNA concentrations than genomic codon-usage frequency, and that specific codons (including ACA) at the 5' end of mRNA molecules could have a significant impact on mRNA stability and subsequent protein levels. Based on the predictions that codons ending in 'A' are generally more favorable and lead to increased protein expression, we postulate that this likely underlies the increased signal accumulation with $DsRed_{42}$.

Recently, we have shown that NO-exposed Hmp^{+} cells preferentially survive doxycycline treatment in our mouse model of infection, which suggested the Hmp^{+} cells may represent a slow growing subpopulation of bacteria [30]. Our *in vitro* results were consistent with this, where exposure to NO was sufficient for $DsRed_{42}$ signal accumulation. Our results are also consistent with a recently published study which showed that NO causes a collapse of proton motive force (PMF) and collapse of the divisome complex, thus resulting in cell division arrest [47]. However, within host tissues, bacterial cells with $DsRed_{42}$ signal accumulation were largely Hmp[-], and instead expressed the stationary phase marker, Dps. We believe this surprising result may be a reflection of the transient bacterial exposure to NO during infection. Consistent with this idea, we found that only a few bacterial cells express the destabilized *hmp* reporter at 72h p.i. (**Fig 8D**). The half-life of this destabilized mCherry protein is approximately 35 minutes in culture [30], and assuming the turnover rate is similar within host tissues, this marks a very recent exposure to NO. This mosaic of expression suggests that while many cumulative cells were exposed to NO and responded with *hmp* expression, this process is transient and actively occurring in only a few cells at a time.

Following transient exposure to NO, bacteria need to repair NO-mediated damage to survive and resume replication [46,54]. We also know repair of Fe-S clusters promotes *Y. pseudotuberculosis* survival after NO exposure, and likely promotes continued bacterial growth after stress [28]. What remains unclear is why Hmp^{+} cells have decreased antibiotic susceptibility, since this does not appear to be linked to slowed cell division rates. Recently, it has been shown that slowed metabolic activity is a better correlate for decreased antibiotic susceptibility

[1], which could mean that Hmp$^+$ cells have decreased metabolic activity even after cell division has resumed. These results could also suggest that Hmp$^+$ cells may change in another way that promotes a tolerance phenotype, possibly by upregulation or downregulation of specific genes or pathways, or utilization of less energetically favorable metabolic pathways, that again lead to decreased metabolic rates. It would also be interesting to visualize the impact of antibiotic treatment on DsRed$_{42}$-expressing populations, to see if DsRed$_{42}$$^+$ *Yersinia* also have decreased antibiotic susceptibility, as you would predict based on results with *Salmonella* [15]. Consistent with this idea, doxycycline treatment at 72h p.i. with *Y. pseudotuberculosis* did not significantly prolong mouse survival, suggesting the DsRed$_{42}$$^+$ cells may be very tolerant to antibiotics [30].

The *in vitro* studies we performed here were used to better characterize the conditions that lead to DsRed$_{42}$ signal accumulation, and compare DsRed$_{42}$ signal to other stress reporters. The results we obtained with NO were expected, based on the role of NO in causing cell division arrest. However, the results comparing DsRed$_{42}$ with the *dps* reporter were less clear, especially as we compared DsRed$_{42}$ and *dps* reporters in culture to the results we observed within host tissues. Based on the results *in vitro*, we believe that *dps* transcript levels begin to accumulate early in the transition into post-exponential and stationary phase. This early increase in transcripts leads to an early accumulation in the stable *dps* reporter signal, prior to the point where growth actually slows. *In vitro* results with the unstable *dps* reporter suggest there is a second wave of *dps* transcription late in stationary phase that correlates with slowed growth and DsRed$_{42}$ signal accumulation. Our *in vivo* results instead show overlap in the stable *dps* reporter signal and DsRed$_{42}$ signal; detection of both signals together lends confidence to the idea that these cells represent a slow-growing subset. However, there are many different conditions that could arise *in vivo* that may promote differential DsRed$_{42}$ signal accumulation, such as low oxygenation or *in vivo* differences in expression levels. The unstable *dps* reporter unfortunately could not be detected within host tissues, likely because the signal was so dim with this reporter construct in general (**Fig 4F**), and because the spleen has relatively high background green fluorescence. Dps protein was also enriched in TIMER^{bac+} *Salmonella* populations [15], again supporting the idea that the Dps$^+$ DsRed$_{42}$$^+$ cells we detected within host tissues are truly slow-growing. Dps regulation is complex, and expression can be triggered by exposure to ROS and iron availability, in addition to RpoS-dependent stationary phase transitions and general nutrient deprivation [55–57]. DsRed$_{42}$, in contrast, should indicate slowed growth and could be used to isolate bacterial subsets to confirm this slowed growth phenotype, and to better understand what stressors are promoting slowed growth. The combination of these two reporters together could be particularly informative in future experiments to determine the mechanisms underlying the formation of slow-growing subsets of bacteria within host tissues.

Materials and methods

Ethics statement

All animal studies were approved by the Institutional Animal Care and Use Committee of Johns Hopkins University. This study does not include human participants or donors.

Bacterial strains & growth conditions. The WT *Y. pseudotuberculosis* strain, IP2666, was used throughout [24,27]. For all mouse infection experiments, bacteria were grown overnight (16h) to post-exponential phase in 2xYT broth (LB, with 2x yeast extract and tryptone) at 26˚C with rotation. For *in vitro* experiments with *hmp* and DsRed$_{42}$ reporters, or *dps* and DsRed$_{42}$ reporters, bacteria were grown overnight (16h) to post-exponential phase in LB prior to experimental set-up. Overnight cultures of *E. coli* were grown in LB with 1mM IPTG at 37˚C with

rotation for 24h prior to cell sorting. 1mM IPTG was used for induction throughout these experiments.

Site-directed and random mutagenesis. Site-directed mutagenesis was used to generate the TIMER$_{I161T\ T197A}$ variant from WT TIMER. Mutations were made sequentially by amplifying across the gene with primers containing the desired mutations. Briefly, TIMER was amplified in two pieces, with the mutation incorporated at the 3' end of the upstream piece, and 5' end of the downstream piece; overlap extension was used to join these homologous fragments [24]. We generated TIMER$_{I161T}$ first, then used this as a template to generate TIMER$_{I161T\ T197A}$. For random mutagenesis, the TIMER$_{I161T\ T197A}$ gene was amplified by PCR to use as a template for random mutagenesis PCR reactions. TIMER$_{I161T\ T197A}$ was then amplified using the Agilent Gene Morph II kit for a single round of random mutagenesis and PCR products were purified (QIAGEN). These products were used as template DNA in an additional PCR reaction, where products were amplified to add restriction enzyme sites onto the 5' and 3' ends (10 cycles). PCR products were purified again before restriction digestion (EcoRI, BamHI), ligation into the *lacZ* gene of pUC18, and electroporation into XL1-BLUE *E. coli*. Transformants were plated onto IPTG/X-gal LB plates to ensure the majority of colonies contained an insert, based on white colony color. Transformants were then grown in culture +IPTG (1mM) for 24h, bacteria were pelleted, resuspended in PBS, and placed on ice during fluorescence-activated cell sorting (MoFlo XDP cell sorter, Beckman Coulter). Bacteria with red fluorescence (approximately 200 cells) were collected and plated onto LB/Amp for single colonies. 192 colonies (two 96 well plates) were screened for red fluorescence after 24h growth in 200μl LB +IPTG at 37˚C with shaking. 26 colonies had clear red fluorescent signal, and pUC18 plasmids were isolated by miniprep (QIAGEN) from these colonies for sequencing.

Generation of reporter strains. Two of the fluorescent constructs in this study were previously described: the constitutive GFP and P_{hmp}::*gfp* (GFPmut3) [24,26]. The final DsRed$_{42}$ plasmid was constructed by amplifying the *hmsT* promoter, fusing this immediately upstream of DsRed$_{42}$, and inserting this into pMMB67EH. The destabilized *gfp* was constructed by fusing an 11 amino acid *ssrA* tag, with AAV terminal amino acids, between the last coding amino acid and the stop codon [42,43]. This was inserted downstream of the P_{tac} IPTG inducible promoter in pMMB207Δ267 [58] to quantify GFP half-life following IPTG induction. A stable *gfp* construct was generated in parallel as a control (**S3 Fig**). The P_{dps}::*gfp* and P_{dps}::*gfp-ssrA* reporters were generated by amplifying the *dps* promoter, fusing this to either stable or destabilized *gfp* by overlap extension PCR, and inserting this into pACYC184 [24]. The P_{hmp}::*gfp-ssrA* reporter was generated by fusing the *hmp* promoter to destabilized *gfp*, and was inserted into pACYC184 [24]. The tandem *hmp* reporter constructs were generated by first fusing either stable or destabilized mCherry to stable *gfp*; these tandems were inserted into pMMB207Δ267 first to quantify mCherry half-life [30]. The *hmp* promoter was then fused to each tandem, and these fragments were inserted into pACYC184. All plasmid transformations into *Y. pseudotuberculosis* were performed using a previously published protocol [59].

DsRed$_{42}$ in vitro experimental design. Individual colonies were inoculated into 200μl LB within individual wells of 96-well, black-walled, clear-bottom plates (Greiner). Surrounding wells were filled with 200μl PBS to prevent evaporation during growth. Plates were covered with aluminum foil to prevent light exposure, and were incubated at 37˚C with shaking for the indicated timepoints. At individual time points fluorescence and absorbance were measured using a plate reader (see below) and aliquoted for fluorescence microscopy. For experiments with *dps* reporter strains, plates were incubated without shaking at 37˚C. For experiments with acidified nitrite, overnight cultures were diluted 1:50 into 200μl fresh LB pH5.5, in the presence or absence of the indicated concentrations of NaNO$_2$, within wells. For experiments with DETA-NONOate, overnight cultures were diluted 1:50 into 200μl fresh LB, in the presence or

absence of 2.5mM DETA-NONOate. Non-fluorescence WT IP2666 was grown alongside reporter strains for all experiments to determine the baseline fluorescence of Yptb grown under the indicated conditions.

Fluorescence detection, plate reader.   Bacterial samples were quantified directly in black-walled, clear bottom, 96 well plates. Optical density (A_{600nm}) was used to approximate cell number by subtracting values from blank media control wells. For Yptb experiments, $DsRed_{42}$ fluorescence was detected with 560nm excitation/610nm emission, and GFP fluorescence was detected with 480nm excitation/520nm emission, using a Synergy H1 microplate reader (Biotek). Fold change represents fluorescence in reporter strains relative to the average value for non-fluorescent WT Yptb. For *E. coli* experiments, TIMER signal was also detected with a spectral curve, with excitation at 480nm, and emission detected between 500nm-600nm.

Fluorescence microscopy: Bacteria.   To visualize individual bacterial cells, 100μl of each sample was taken from 96 well plates and pelleted, resuspended in 100μl 4% PFA, and incubated at 4°C for 30 minutes for fixation. PFA was removed and bacteria were resuspended in 25μl PBS prior to imaging. Agarose pads were prepared to immobilize bacteria for imaging, by solidifying a thin layer of 25μl 1% agarose in PBS between a microscope slide and coverslip. Once solidified, coverslips were removed, bacteria (8μl) were added, coverslips were replaced, and bacteria were imaged with the 63x oil immersion objective, using a Zeiss Axio Observer. Z1 (Zeiss) fluorescent microscope with Colibri.2 LED light source and an ORCA-R^2 digital CCD camera (Hamamatsu). Volocity image analysis software was used to specifically select individual bacterial cells and quantify the fluorescent signal associated with each cell.

Murine model of systemic infection.   Six to 8-week old female C57BL/6 mice were obtained from Jackson Laboratories (Bar Harbor, ME). All animal studies were approved by the Institutional Animal Care and Use Committee of Johns Hopkins University. Mice were injected intravenously into the tail vein with 10^3 bacteria for all experiments [24,28,30]. At the indicated timepoints post-inoculation (p.i.), spleens were removed and processed. Intact tissue was fixed for fluorescence microscopy. Tissue was homogenized to quantify CFUs.

Fluorescence microscopy: Host tissues.   Spleens were harvested and immediately fixed in 4% PFA in PBS for either 3 hours at room temperature or 24 hours at 4°C. Tissues were frozen-embedded in Sub Xero freezing media (Mercedes Medical) and cut by cryostat microtome (Microm HM 505e) into 10μm sections. To visualize reporters, sections were thawed in PBS, stained with Hoechst at a 1:10,000 dilution, washed in PBS, and coverslips were mounted using ProLong Gold (Life Technologies). In **Fig 3**, neutrophils were also detected by immuno-fluorescence microscopy; sections were thawed, permeabilized with ice-cold 100% methanol and blocked in 2% BSA in PBS. Neutrophils were detected using a rat anti-mouse Ly6G unconjugated antibody (BD) and goat anti-rat Alexa 350-conjugated secondary antibody (Invitrogen). Sections were incubated with primary antibodies, washed, incubated with secondary antibodies, washed, and coverslips were mounted with ProLong Gold. Tissue was imaged as described above, with an Apotome.2 (Zeiss) for optical sectioning.

qRT-PCR to detect bacterial transcripts in broth-grown cultures.   Bacterial cells were grown in the presence or absence of DETA-NONOate for 4 hours, pelleted, resuspended in Buffer RLT (QIAGEN) + ß-mercaptoethanol, and RNA was isolated using the RNeasy kit (QIAGEN) according to manufacturer's protocol. DNA contamination was eliminated using the DNA-free kit (Ambion). RNA was reverse transcribed using M-MLV reverse transcriptase (Invitrogen), in the presence of the RNase inhibitor, RnaseOUT (Invitrogen). Approximately 30 ng cDNA was used as a template in reactions with 0.5 μM of forward and reverse primers [24] and SYBR Green (Applied Biosystems). Control samples were prepared that lacked M-MLV, to confirm DNA was eliminated from samples. Reactions were carried out using the

StepOnePlus Real-Time PCR system, and relative comparisons were obtained using the $\Delta\Delta C_T$ or $2^{-\Delta Ct}$ method (Applied Biosystems). Kits were used according to manufacturers' protocols.

Image analysis. Volocity image analysis software was used to quantify microcolony areas and fluorescence as previously described [24]. Image J was used to quantify the signal intensity of each channel at the centroid and periphery of each microcolony, to generate relative signal intensities of fluorescent reporters, as previously described [24,30]. Thresholding was used to define the total area and centroid of each microcolony, and 0.01 pixel^2 squares were selected to calculate values. Peripheral measurements depict bacteria in contact with host cells [24,30].

Statistical analyses for correlations. To determine if fluorescent signals were correlated, we performed linear regression analysis and are depicting best-fit lines. R^2 values are shown to depict whether there is a linear correlation between the two fluorescent signals, however strength of correlation was assessed based on whether the slope of the best fit line was significantly non-zero. Low R^2 values for many of the correlations are due to significant differences in the magnitude of fluorescent signals; DsRed$_{42}$ signal is low relative to transcriptional fluorescent reporters. Additional statistical analyses were performed as described in figure legends.

Supporting information

S1 Fig. *TIMER$_{I161T\ T197A}$* lacks fluorescence. The indicated strains contain the *TIMER$_{I161T}$ $_{T197A}$* variant in the low copy vector, pMMB67EH. Strains were grown at 37˚C in 96 well plates with shaking for 24h. Fluorescence was detected with a spectral curve with excitation at 480nm and emission detected between 500nm-600nm. Relative fluorescence units (RFUs) represent raw values with media only background subtracted, data represents mean of three biological replicates. A) *E. coli* strains: *E. coli* is the non-fluorescent DH5αλpir *E. coli* parent strain. B) *Y. pseudotuberculosis* strains: Yptb is the non-fluorescent WT IP2666 parent strain. (TIF)

S2 Fig. Red fluorescence emerges in DsRed variants. *E. coli* strains (XLI-BLUE background) contain the indicated DsRed variants, expressed from the high copy pUC18 plasmid. Strains were grown for the indicated times at 37˚C in 96 well plates with shaking. Fluorescence was detected with a spectral curve with excitation at 480nm and emission detected between 500nm-600nm. Relative fluorescence units (RFUs) represent raw values with media only background subtracted, data represents mean of three biological replicates. A) Optical density of the indicated strains was measured by absorbance (A_{600nm}) over time (hours, h), during incubation at 37˚C in a plate reader. B) The indicated strains were grown as described above, and optical density was measured by absorbance (A_{600nm}) at the indicated timepoints (hours, h) C) DsRed variants were grown alongside the non-fluorescent WT *E. coli* strain in the presence of IPTG for the indicated times. *E. coli* +IPTG: 24h growth. D) DsRed variants grown alongside the non-fluorescent WT *E. coli* strain, in the presence or absence of IPTG for 24h. Vertical dotted lines: 520nm (green fluorescence) and 580nm (red fluorescence). Statistics: A)- B) Two-way ANOVA with Tukey's multiple comparison test; n.s.: not-significant. (TIF)

S3 Fig. Stability of GFP and GFP-ssrA. WT IP2666 containing IPTG-inducible *gfp* or *gfp-ssrA* were grown overnight (16h) in the presence of IPTG. Cells were pelleted and resuspended in PBS, and kanamycin was added to inhibit additional protein translation. GFP signal was detected with 480nm excitation/520nm emission every 5 minutes for 120 minutes in a plate reader, to detect the half-life of each fluorescent protein by the one-phase exponential decay equation. Fluorescent values are expressed as % of signal (GFP), where time 0 equals 100% signal intensity and 0% signal intensity indicates the limit of detection. Data represents mean of

three biological replicates.
(TIF)

Acknowledgments

We thank the members of the Davis lab, who provided feedback and suggestions during the final steps of manuscript preparation. We also thank Dr. Ralph R. Isberg for guidance and feedback throughout this project.

Author Contributions

Conceptualization: Pavan Patel, Brendan J. O'Hara, Emily Aunins, Kimberly M. Davis.

Formal analysis: Pavan Patel, Kimberly M. Davis.

Funding acquisition: Kimberly M. Davis.

Investigation: Pavan Patel, Brendan J. O'Hara, Kimberly M. Davis.

Methodology: Pavan Patel, Brendan J. O'Hara, Emily Aunins, Kimberly M. Davis.

Writing – original draft: Pavan Patel, Kimberly M. Davis.

Writing – review & editing: Pavan Patel, Brendan J. O'Hara, Emily Aunins, Kimberly M. Davis.

References

1. Lopatkin A, Stokes J, Zheng E, Yang J, Takahashi M, You L, et al. Bacterial metabolic state more accurately predicts antibiotic lethality than growth rate. Nat Microbiol. 2019; 4(12):2109–17. https://doi.org/10.1038/s41564-019-0536-0 PMID: 31451773

2. Stewart P, White B, Boegli L, Hamerly T, Williamson K, Franklin M, et al. Conceptual model of biofilm antibiotic tolerance that integrates phenomena of diffusion, metabolism, gene expression, and physiology. J Bacteriol. 2019; 201(22):e00307–19. https://doi.org/10.1128/JB.00307-19 PMID: 31501280

3. Cohen N, Lobritz M, Collins J. Microbial persistence and the road to drug resistance. Cell Host Microbe. 2013; 13(6):632–42. https://doi.org/10.1016/j.chom.2013.05.009 PMID: 23768488

4. Terskikh A, Fradkov A, Zaraisky A, Kajava A, Angres B. Analysis of DsRed Mutants. Space around the fluorophore accelerates fluorescence development. J Biol Chem. 2002; 277(10):7633–6. https://doi.org/10.1074/jbc.C100694200 PMID: 11773062

5. Verkhusha V, Otsuna H, Awasaki T, Oda H, Tsukita S, Ito K. An enhance mutant of red fluorescent protein DsRed for double labeling developmental timer of neural fiber bundle formation. J Biol Chem. 2001; 276(32):29621–4. https://doi.org/10.1074/jbc.C100200200 PMID: 11408473

6. Helaine S, Thompson J, Watson K, Liu M, Boyle C, Holden D. Dynamics of intracellular bacterial replication at the single cell level. Proc Natl Acad Sci. 2010; 107(8):3746–51. https://doi.org/10.1073/pnas.1000041107 PMID: 20133586

7. Roostalu J, Jöers A, Luidalepp H, Kaldalu N, Tenson T. Cell division in *Escherichia coli* cultures monitored at single cell resolution. BMC Microbiol. 2008; 8:68. https://doi.org/10.1186/1471-2180-8-68 PMID: 18430255

8. Kaiser P, Regoes R, Dolowschiak T, Wotzka S, Lengefeld J, Slack E, et al. Cecum lymph node dendritic cells harbor slow-growing bacteria phenotypically tolerant to antibiotic treatment. PLoS Biol. 2014; 12 (2). https://doi.org/10.1371/journal.pbio.1001793 PMID: 24558351

9. Reyes-Lamothe R, Sherratt D, Leake M. Stoichiometry and architecture of active DNA replication machinery in *Escherichia coli*. Science. 2010; 328(5977):498–501. https://doi.org/10.1126/science.1185757 PMID: 20413500

10. Sukumar N, Tan S, Aldridge B, Russell D. Exploitation of *Mycobacterium tuberculosis* reporter strains to probe the impact of vaccination at sites of infection. PLoS Pathog. 2014; 10(9):e1004394. https://doi.org/10.1371/journal.ppat.1004394 PMID: 25233380

11. Liechti G, Kuru E, Hall E, Kalinda A, Brun Y, VanNieuwenhze M, et al. A new metabolic cell-wall labeling method reveals peptidoglycan in *Chlamydia trachomatis*. Nature. 2014; 506(7489):507–10. https://doi.org/10.1038/nature12892 PMID: 24336210

12. Siegrist M, Swarts B, Fox D, Lim S, Bertozzi C. Illumination of growth, division and secretion by metabolic labeling of the bacterial cell surface. FEMS Microbiol Rev. 2015; 39(2):184–202. https://doi.org/10.1093/femsre/fuu012 PMID: 25725012

13. Gonzalez R, Lane M, Wagner N, Weening E, Miller V. Dissemination of a highly virulent pathogen: tracking the early events that define infection. PLoS Pathog. 2015; 11(1):e1004587. https://doi.org/10.1371/journal.ppat.1004587 PMID: 25611317

14. McVicker G, Prajsnar T, Williams A, Wagner N, Boots M, Renshaw S, et al. Clonal expansion during *Staphylococcus aureus* infection dynamics reveals the effect of antibiotic intervention. PLoS Pathog. 2014; 10(2):e1003959. https://doi.org/10.1371/journal.ppat.1003959 PMID: 24586163

15. Claudi B, Spröte P, Chirkova A, Personnic N, Zankl J, Schürmann N, et al. Phenotypic variation of *Salmonella* in host tissues delays eradication by antimicrobial chemotherapy. Cell. 2014; 158(4):722–33. https://doi.org/10.1016/j.cell.2014.06.045 PMID: 25126781

16. Strack R, Strongin D, Mets L, Glick B, Keenan R. Chromophore formation in DsRed occurs by a branched pathway. J Am Chem Soc. 2010; 132(24):8496–505. https://doi.org/10.1021/ja1030084 PMID: 20509651

17. Terskikh A, Fradkov A, Ermakova G, Zaraisky A, Tan P, Kajava A, et al. "Fluorescent timer": protein that changes color with time. Science. 2000; 290(5496):1585–8. https://doi.org/10.1126/science.290.5496.1585 PMID: 11090358

18. Rang C, Galen J, Kaper J, Chao L. Fitness cost of the green fluorescent protein in gastrointestinal bacteria. Can J Microbiol. 2003; 49(9):531–7. https://doi.org/10.1139/w03-072 PMID: 14608419

19. Gemski P, Lazere J, Casey T. Plasmid associated with pathogenicity and calcium dependency of *Yersinia enterocolitica*. Infect Immun. 1980; 27(2):682–5. https://doi.org/10.1128/iai.27.2.682-685.1980 PMID: 7380546

20. Luk C, Valenzuela C, Gil M, Swistak L, Bomme P, Chang Y, et al. *Salmonella* enters a dormant state within human epithelial cells for persistent infection. PLoS Pathog. 2021; 17(4). https://doi.org/10.1371/journal.ppat.1009550 PMID: 33930101

21. Personnic N, Streidnig B, Lezan E, Manske C, Welin A, Schmidt A, et al. Quorum sensing modulates the formation of virulent *Legionella* persisters within infected cells. Nat Commun. 2019; 10(1). https://doi.org/10.1038/s41467-019-13021-8 PMID: 31740681

22. Peterson L, Philip N, DeLaney A, Wynosky-Dolfi M, Asklof K, Gray F, et al. RIPK1-dependent apoptosis bypasses pathogen blockage of innate signaling to promote immune defense. J Exp Med. 2017; 214(11):3171–82. https://doi.org/10.1084/jem.20170347 PMID: 28855241

23. Zhang Y, Khairallah C, Sheridan B, van der Velden A, Bliska J. CCR2+ inflammatory monocytes are recruited to *Yersinia pseudotuberculosis* pyogranulomas and dictate adaptive responses at the expense of innate immunity during oral infection. Infect Immun. 2018; 86(3):e00782–17. https://doi.org/10.1128/IAI.00782-17 PMID: 29263104

24. Davis K, Mohammadi S, Isberg R. Community behavior and spatial regulation within a bacterial microcolony in deep tissue sites serves to protect against host attack. Cell Host Microbe. 2015; 17(1):21–31. https://doi.org/10.1016/j.chom.2014.11.008 PMID: 25500192

25. Balada-Llasat J, Mecsas J. Yersinia has a tropism for B and T cell zones of lymph nodes that is independent of the type III secretion system. PLoS Pathog. 2006; 2(9):e86. https://doi.org/10.1371/journal.ppat.0020086 PMID: 16948531

26. Crimmins G, Mohammadi S, Green E, Bergman M, Isberg R, Mecsas J. Identification of MrtAB, an ABC transporter specifically required for *Yersinia pseudotuberculosis* to colonize the mesenteric lymph nodes. PLoS Pathog. 2012; 8(8):e1002828. https://doi.org/10.1371/journal.ppat.1002828 PMID: 22876175

27. Green E, Clark S, Crimmins G, Mack M, Kumamoto C, Mecsas J. Fis is essential for *Yersinia pseudotuberculosis* virulence and protects against reactive oxygen species produced by phagocytic cells during infection. PLoS Pathog. 2016; 12(9):e1005898. https://doi.org/10.1371/journal.ppat.1005898 PMID: 27689357

28. Davis K, Krupp J, Clark S, Isberg R. Iron-sulfur cluster repair contributes to *Yersinia pseudotuberculosis* survival within deep tissues. Infect Immun. 2019; 87(10). https://doi.org/10.1128/IAI.00533-19 PMID: 31331956

29. Poole R, Anjum M, Membrillo-Hernández J, Kim S, Hughes M, Stewart V. Nitric oxide, nitrite, and Fnr regulation of *hmp* (flavohemoglobin) gene expression in *Escherichia coli* K-12. J Bacteriol. 1996; 178(18):5487–92. https://doi.org/10.1128/jb.178.18.5487-5492.1996 PMID: 8808940

30. Raneses J, Ellison A, Liu B, Davis K. Subpopulations of stressed *Y. pseudotuberculosis* preferentially survive doxycycline treatment within host tissues. mBio. 2020; 11(4):e00901–20. https://doi.org/10.1128/mBio.00901-20 PMID: 32753491

31. Boël G, Letso R, Neely H, Price W, Wong K, Su M, et al. Codon influences on protein expression in *E. coli* correlates with mRNA levels. Nature. 2016; 529(7586):358–63. https://doi.org/10.1038/nature16509 PMID: 26760206

32. Jones H, Lillard J, Perry R. HmsT, a protein essential for expression of the haemin storage (Hms+) phenotype of *Yersinia pestis*. Microbiology. 1999; 145:2117–28. https://doi.org/10.1099/13500872-145-8-2117 PMID: 10463178

33. Sun Y, Koumoutsi A, Jarrett C, Lawrence K, Gherardini F, Darby C, et al. Differential control of *Yersinia pestis* biofilm formation in vitro and in the flea vector by two c-di-GMP diguanylate cyclases. PLoS One. 2011; 6(4). https://doi.org/10.1371/journal.pone.0019267 PMID: 21559445

34. Rollenhagen C, Bumann D. *Salmonella enterica* highly expressed genes are disease specific. Infect Immun. 2006; 74(3):1649–60. https://doi.org/10.1128/IAI.74.3.1649-1660.2006 PMID: 16495536

35. Rollenhagen C, Sörensen M, Rizos K, Hurvitz R, Bumann D. Antigen selection based on expression levels during infection facilitates vaccine development for an intracellular pathogen. Proc Natl Acad Sci. 2004; 101(23):8739–44. https://doi.org/10.1073/pnas.0401283101 PMID: 15173591

36. Hecht A, Glasgow J, Jaschke P, Bawazer L, Munson M, Cochran J, et al. Measurements of translation initiation from all 64 codons in *E. coli*. Nucleic Acids Res. 2017; 45(7):3615–26. https://doi.org/10.1093/nar/gkx070 PMID: 28334756

37. Cunrath O, Bumann D. Host resistance factor SLC11A1 restricts *Salmonella* growth through magnesium deprivation. Science. 2019; 366(6468):995–9. https://doi.org/10.1126/science.aax7898 PMID: 31753999

38. Subach F, Subach O, Gundorov I, Morozova K, Piatkevich K, Cuervo A, et al. Monomeric fluorescent timers that change color from blue to red report on cellular trafficking. Nat Chem Biol. 2009; 5(2):118–26. https://doi.org/10.1038/nchembio.138 PMID: 19136976

39. Strack R, Strongin D, Bhattacharyya D, Tao W, Berman A, Broxmeyer H, et al. A noncytotoxic DsRed variant for whole-cell labeling. Nat Methods. 2008; 5(11):955–7. https://doi.org/10.1038/nmeth.1264 PMID: 18953349

40. Almiron M, Link A, Furlong D, Kolter R. A novel DNA-binding protein with regulatory and protective roles in starved *Escherichia coli*. Genes Dev. 1992; 6(12B):2646–54. https://doi.org/10.1101/gad.6.12b.2646 PMID: 1340475

41. Nair S, Finkel S. Dps protects cells against multiple stresses during stationary phase. J Bacteriol. 2004; 186(13):4192–8. https://doi.org/10.1128/JB.186.13.4192-4198.2004 PMID: 15205421

42. Andersen J, Sternberg C, Poulsen L, Bjorn S, Givskov M, Molin S. New unstable variants of green fluorescent protein for studies of transient gene expression in bacteria. Appl Environ Microbiol. 1998; 64(6):2240–6. https://doi.org/10.1128/AEM.64.6.2240-2246.1998 PMID: 9603842

43. Keiler K, Waller P, Sauer R. Role of a peptide tagging system in degradation of proteins synthesized from damaged messenger RNA. Science. 1996; 271(5251):990–3. https://doi.org/10.1126/science.271.5251.990 PMID: 8584937

44. Dykhuizen R, Frazer R, Duncan C, Smith C, Golden M, Benjamin N, et al. Antimicrobial effect of acidified nitrite on gut pathogens: importance of dietary nitrate in host defense. Antimicrob Agents Chemother. 1996; 40(6):1422–5. https://doi.org/10.1128/AAC.40.6.1422 PMID: 8726013

45. Clark S, Thibault D, Shull L, Davis K, Aunins E, van Opijnen T, et al. Topologically correct synthetic reconstruction of pathogen social behavior found in deep tissue sites. eLife. 2020; 9. https://doi.org/10.7554/eLife.58106 PMID: 32543373

46. Fang F, Vázquez-Torres A. Reactive nitrogen species in host-bacterial interactions. Curr Opin Immunol. 2019; 60:96–102. https://doi.org/10.1016/j.coi.2019.05.008 PMID: 31200187

47. Jones-Carson J, Yahashiri A, Kim J, Liu L, Fitzsimmons L, Weiss D, et al. Nitric oxide disrupts bacterial cytokinesis by poisoning purine metabolism. Sci Adv. 2020; 6(9). https://doi.org/10.1126/sciadv.aaz0260 PMID: 32133408

48. Strack R, Bhattacharyya D, Glick B, Keenan R. Noncytotoxic orange and red/green derivatives of DsRed-Express2 for whole-cell labeling. BMC Biotechnol. 2009;9. https://doi.org/10.1186/1472-6750-9-9 PMID: 19220883

49. Strack R, Hein B, Bhattacharyya D, Hell S, Keenan R, Glick B. A rapidly maturing far-red derivative of DsRed-Express2 for whole-cell labeling. Biochemistry. 2009; 48(35):8279–81. https://doi.org/10.1021/bi900870u PMID: 19658435

50. Schulte M, Olschewski K, Hensel M. Fluorescent protein-based reporters reveal stress response of intracellular *Salmonella enterica* at level of single bacterial cells. Cell Microbiol. 2021; 23(3). https://doi.org/10.1111/cmi.13293 PMID: 33222378

51. Saliba A, Li L, Westermann A, Appenzeller S, Stapels D, Schulte L, et al. Single-cell RNA-seq ties macrophage polarization to growth rate of intracellular *Salmonella*. Nat Microbiol. 2016;2. https://doi.org/10.1038/nmicrobiol.2016.206 PMID: 27841856

52. Stapels D, Hill P, Westermann A, Fisher R, Thurston T, Saliba A, et al. *Salmonella* persisters undermine host immune defenses during antibiotic treatment. Science. 2018; 362:1156–60. https://doi.org/10.1126/science.aat7148 PMID: 30523110

53. Zoubeidi A, Schwiesow L, Auerbuch V, Lam H. Complete genome assembly of *Yersinia pseudotuberculosis* IP2666pIB1. Microbiol Resour Announc. 2019; 8(7):e01592–18. https://doi.org/10.1128/MRA.01592-18 PMID: 30801065

54. Poole R. Nitric oxide and nitrosative stress tolerance in bacteria. Biochem Soc Trans. 2005; 33:176–80. https://doi.org/10.1042/BST0330176 PMID: 15667299

55. De Martino M, Ershov D, van den Berg P, Tans S, Meyer A. Single-Cell Analysis of the Dps Response to Oxidative Stress. J Bacteriol. 2016; 198(11):1662–74. https://doi.org/10.1128/JB.00239-16 PMID: 27021559

56. Calhoun L, Kwon Y. Structure, function and regulation of the DNA-binding protein Dps and its role in acid and oxidative stress resistance in *Escherichia coli*: a review. J Appl Microbiol. 2011; 110(2):375–86. https://doi.org/10.1111/j.1365-2672.2010.04890.x PMID: 21143355

57. Karas V, Westerlaken I, Meyer A. The DNA-Binding Protein from Starved Cells (Dps) Utilizes Dual Functions To Defend Cells against Multiple Stresses. J Bacteriol. 2015; 197(19):3206–15. https://doi.org/10.1128/JB.00475-15 PMID: 26216848

58. O'Connor T, Boyd D, Dorer M, Isberg R. Aggravating genetic interactions allow a solution to redundancy in a bacterial pathogen. Science. 2012; 338(6113):1440–4. https://doi.org/10.1126/science.1229556 PMID: 23239729

59. Davidson R, Davis K. *Yersinia pseudotuberculosis*: Cultivation, Storage, and Methods for Introducing DNA. Curr Protoc Microbiol. 2020; 59(1).